cmgh
CELLULAR AND MOLECULAR GASTROENTEROLOGY AND HEPATOLOGY

ORIGINAL RESEARCH

Intestinal α1-2-Fucosylation Contributes to Obesity and Steatohepatitis in Mice

Rongrong Zhou,[1,2,*] Cristina Llorente,[2,*] Jinling Cao,[2,3] Livia S. Zaramela,[4] Suling Zeng,[2,5] Bei Gao,[2] Shang-Zhen Li,[5] Ryan D. Welch,[6] Feng-Qing Huang,[7] Lian-Wen Qi,[7] Chuyue Pan,[8] Yan Huang,[1] Pengchen Zhou,[1] Iris Beussen,[9] Ying Zhang,[9,10] Gregory Bryam,[9] Oliver Fiehn,[9] Lirui Wang,[8] E-Hu Liu,[5] Ruth T. Yu,[6] Michael Downes,[6] Ronald M. Evans,[6] Karrie Goglin,[11] Derrick E. Fouts,[12] David A. Brenner,[2] Lars Bode,[13] Xuegong Fan,[1] Karsten Zengler,[4,14] and Bernd Schnabl[2,15]

[1]Department of Infectious Diseases, Xiangya Hospital, Central South University and Key Laboratory of Viral Hepatitis, Hunan, Changsha, China; [2]Department of Medicine, [4]Department of Pediatrics, [13]Department of Pediatrics and Larsson-Rosenquist Foundation Mother-Milk-Infant Center of Research Excellence, [14]Department of Bioengineering, University of California San Diego, La Jolla, California; [3]College of Food Science and Engineering, Shanxi Agricultural University, Shanxi, Taigu, China; [5]State Key Laboratory of Natural Medicines, [7]The Clinical Metabolomics Center, [8]School of Basic Medicine and Clinical Pharmacy, China Pharmaceutical University, Nanjing, Jiangsu, China; [6]Gene Expression Laboratory, Salk Institute for Biological Studies, San Diego, California; [9]National Institutes of Health West Coast Metabolomics Center, [10]Department of Chemistry, University of California, Davis, California; [11]J. Craig Venter Institute, La Jolla, California; [12]J. Craig Venter Institute, Rockville, Maryland; [15]Department of Medicine, VA San Diego Healthcare System, San Diego, California

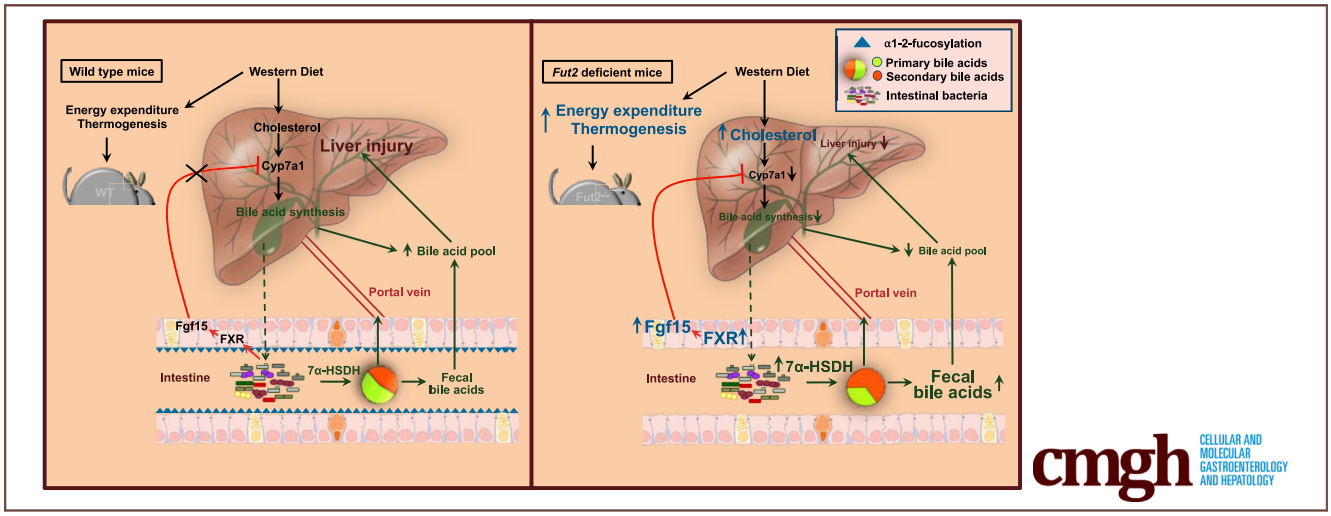

SUMMARY

Intestinal α1-2-fucosylation mediates host–microbe interactions and can shape the metabolism of intestinal microorganisms. Here, we identified that mice lacking α1-2-fucosylation were protected from Western diet–induced features of obesity and steatohepatitis and this protection was mediated through the intestinal microbiota.

BACKGROUND & AIMS: Fucosyltransferase 2 (Fut2)-mediated intestinal α1- 2-fucosylation is important for host–microbe interactions and has been associated with several diseases, but its role in obesity and hepatic steatohepatitis is not known. The aim of this study was to investigate the role of Fut2 in a Western-style diet–induced mouse model of obesity and steatohepatitis.

METHODS: Wild-type (WT) and *Fut2*-deficient littermate mice were used and features of the metabolic syndrome and steatohepatitis were assessed after 20 weeks of Western diet feeding.

RESULTS: Intestinal α1-2-fucosylation was suppressed in WT mice after Western diet feeding, and supplementation of α1-2-fucosylated glycans exacerbated obesity and steatohepatitis in these mice. *Fut2*-deficient mice were protected from Western diet–induced features of obesity and steatohepatitis despite an increased caloric intake. These mice have increased energy expenditure and thermogenesis, as evidenced by a higher core body temperature. Protection from obesity and steatohepatitis

associated with *Fut2* deficiency is transmissible to WT mice via microbiota exchange; phenotypic differences between Western diet–fed WT and *Fut2*-deficient mice were reduced with antibiotic treatment. *Fut2* deficiency attenuated diet-induced bile acid accumulation by altered relative abundance of bacterial enzyme 7-α-hydroxysteroid dehydrogenases metabolizing bile acids and by increased fecal excretion of secondary bile acids. This also was associated with increased intestinal farnesoid X receptor/fibroblast growth factor 15 signaling, which inhibits hepatic synthesis of bile acids. Dietary supplementation of α1-2-fucosylated glycans abrogates the protective effects of *Fut2* deficiency.

CONCLUSIONS: α1-2-fucosylation is an important host-derived regulator of intestinal microbiota and plays an important role for the pathogenesis of obesity and steatohepatitis in mice. *(Cell Mol Gastroenterol Hepatol 2021;12:293–320; https://doi.org/10.1016/j.jcmgh.2021.02.009)*

Keywords: Metabolic Syndrome; Nonalcoholic Steatohepatitis; Microbiota; Metabolome; Bile Acids.

Worldwide obesity has nearly tripled since 1975, and more than 1.9 billion adults were overweight, and among them more than 650 million were obese in 2016.[1,2] Nonalcoholic fatty liver disease (NAFLD), which is associated commonly with obesity, has become a leading cause of chronic liver disease and is one of the main causes for obesity-related deaths.[3,4] Nonalcoholic steatohepatitis (NASH), characterized by hepatic steatosis with inflammation and fibrosis, is the most serious form of NAFLD and can progress to cirrhosis and hepatocellular carcinoma.[5] The pathogenesis of obesity and NASH involves a complex interaction and cross-talk between environmental factors, host genetics, and intestinal microbiota.[6,7]

The enzyme fucosyltransferase 2 (Fut2) encoded by the α1-2-fucosyltransferase 2 gene (*Fut2*) catalyzes the process of α1-2-fucosylation, which adds fucose to glycolipids and glycoproteins, as well as unconjugated glycans such as human milk oligosaccharides.[8–10] In human beings and mice, Fut2 is expressed mainly in epithelial cells of the digestive (intestine and gallbladder) and genital tract, whereas it is absent in liver and adipose tissues. Fut2 is highly expressed in the distal gut where abundant symbiotic microbes are colonizing.[11] Fucosylated glycans are important for host–microbe interactions.[12] Membrane and secreted α1-2-linked fucose can be cleaved by bacterial fucosidase and the liberated L-fucose is used by certain bacteria. L-fucose can serve as substrate for bacteria for the synthesis of fucosylated polysaccharides, regulation of gene expression through the fucose operon, and undergoing catabolism for energy.[13] Epithelial α1-2-fucosylation also can be regulated by microbes because germ-free mice have impaired α1-2-fucosylation in the intestine, which can be restored by colonization with commensal microbes.[14,15] Systemic exposure to Toll-like receptor ligands induces rapid α1-2-fucosylation of epithelial cells in the small intestine.[16]

Intestinal α1-2-fucosylation has been implicated in the pathogenesis of several diseases that are associated with the intestinal microbiome, including Crohn's disease,[17] chronic pancreatitis, primary sclerosing cholangitis, and several infectious diseases.[18] In this study, we investigated whether changes of intestinal α1-2-fucosylation affect Western diet–induced obesity and steatohepatitis in mice.

Results

Feeding a Western Diet Reduces Intestinal α1-2-Fucosylation in Mice

Fut2 is highly expressed in the distal intestinal tract (Figure 1*A*). Fut2 mediates α1-2- fucosylation of proteins and lipids on the surface of intestinal epithelial cells and the gallbladder (Figure 1*B*).[8,9,13] Fut4 and Fut8 mediate α1-3- and α1-6-fucosylation, respectively, and also are expressed in mouse intestine, but to a lesser degree than Fut2. To evaluate the role of intestinal fucosylation for obesity and steatohepatitis, we first compared expression of *Fut2*, *Fut4*, and *Fut8* genes and α1-2-, α1-3-, and α1-6-fucosylated glycans in ileum and colon, in control diet and in Western diet–fed wild-type (WT) mice. Consistent with previous studies, Fut2 was more abundant in the colon compared with the ileum in mice fed a control diet (Figure 2*A*). Both *Fut2* messenger RNA (mRNA) and α1-2-fucosylated glycans were significantly lower after Western diet feeding for 20 weeks as evidenced by quantitative reverse-transcription polymerase chain reaction (PCR) and immunohistochemistry staining (Figure 2*A* and *D*). Although *Fut8* mRNA was up-regulated in colon tissue after Western diet feeding (Figure 2*C*), expression of colonic α1-6-fucosylated glycans was not changed (Figure 2*D*). *Fut4* mRNA and α1-3-fucosylated glycans were not changed in colons of mice fed a Western diet (Figure 2*B* and *D*). These results indicate that colonic Fut2-mediated α1-2-fucosylation is reduced in a Western diet–induced obesity and steatohepatitis mouse model.

To restore intestinal α1-2-fucosylation, we supplemented WT mice with 2'-fucosyllactose (2'-FL) in the drinking water. 2'-FL is a prebiotic commonly found in human milk that cannot be used by the host. Intestinal bacteria can cleave 2'-FL and release L-fucose.[19] Supplementation of 2'-FL resulted in increased body and liver weight, more liver

***Authors share co-first authorship.**

Abbreviations used in this paper: **2'-FL, 2'-fucosyllactose; 7α-HSDH, 7α-hydroxysteroid dehydrogenases; ALT, alanine aminotransferase; bp, base pair; BW, body weight; CA, cholic acid; Cyp7a1, cytochrome P450, family 7, subfamily a, polypeptide 1; DCA, deoxycholic acid; ESI, electrospray ionization; Fgf, fibroblast growth factor; Fut, fucosyltransferase; FXR, farnesoid X receptor; GCA, glycocholic acid; HPLC, high-performance liquid chromatography; LC, liquid chromatography; mRNA, messenger RNA; MS, mass spectrometry; NAFLD, nonalcoholic fatty liver disease; NASH, nonalcoholic steatohepatitis; PCR, polymerase chain reaction; RSD, relative standard deviation; T-β-MCA, tauro-β-muricholic acid; TCA, taurocholic acid; Ucp1, uncoupling protein 1; VCO_2, carbon dioxide production; Vo_2, oxygen consumption; WT, wild type.**

Most current article

2352-345X
https://doi.org/10.1016/j.jcmgh.2021.02.009

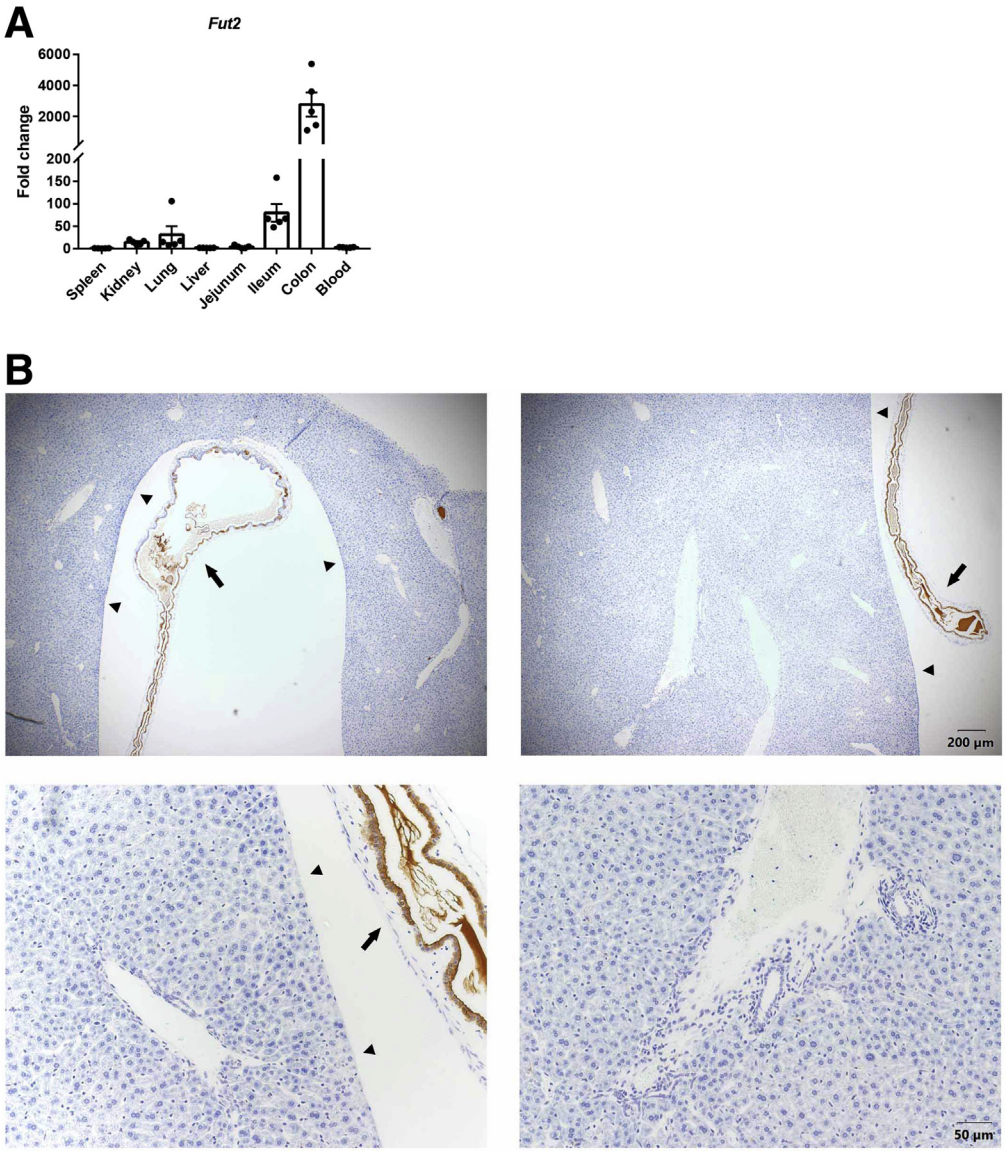

Figure 1. α1-2-fucosylation in different organs in WT mice. WT C57BL/6 mice were fed with chow diet and regular water. (*A*) Expression of *Fut2* mRNA in different organs. (*B*) Representative images of liver (*arrowheads*) and gallbladder (*arrows*) stained for α1-2-fucosylated glycans (Ulex Europaeus Agglutinin I). Experiments were performed in n = 5 from 2 experiments.

injury (as evidenced by higher alanine aminotransferase [ALT] levels), and hepatic steatosis in Western diet–fed but not control diet–fed mice (Figure 2*E*). This raises the possibility that the down-regulation of α1-2-fucosylation in Western diet–fed mice is a protective mechanism.

Fut2-*Deficient Mice Are Protected From Western Diet–Induced Obesity and Metabolic Syndrome*

To further study the role of α1-2-fucosylation for pathogenesis of diet-induced obesity and steatohepatitis, *Fut2*$^{-/-}$ and WT littermate mice were subjected to feeding of a Western diet for 20 weeks. We confirmed that *Fut2*$^{-/-}$ mice lacked expression of α1-2-fucosylated glycans in the intestine by immunohistochemistry staining (Figure 3). *Fut2*$^{-/-}$ mice gained significantly less body weight compared with WT mice (Figure 4*A*). *Fut2* deficiency did not affect epididymal white adipose tissue weight or brown adipose tissue weight (Figure 5*A*). *Fut2*$^{-/-}$ mice showed improved metabolic and endocrine profiles including increased insulin sensitivity and lower plasma levels of cholesterol and leptin compared with WT mice after a Western diet (Figure 4*B–D*). We noticed that Western diet–fed *Fut2*$^{-/-}$ mice had a significantly higher caloric intake than WT littermate mice (Figure 4*E*). Therefore, we restricted the total caloric intake of *Fut2*$^{-/-}$ mice to make it equal to the caloric intake of WT mice during Western diet feeding for 20 weeks. Calorie-restricted *Fut2*$^{-/-}$ mice were fully protected from features of the metabolic syndrome as evidenced by lower body weight and brown adipose tissue, increased insulin sensitivity, and lower levels of plasma cholesterol and leptin than *Fut2*$^{-/-}$ mice with unrestricted access to a Western diet (Figures 4*A–D* and 5*A*).

There was no difference in fecal lipid content during Western diet feeding, indicating that *Fut2*$^{-/-}$ mice have similar levels of intestinal lipid absorption (Figure 5*B*). We compared the metabolic rates of WT and *Fut2*$^{-/-}$ mice on different diets, and no difference was found in control

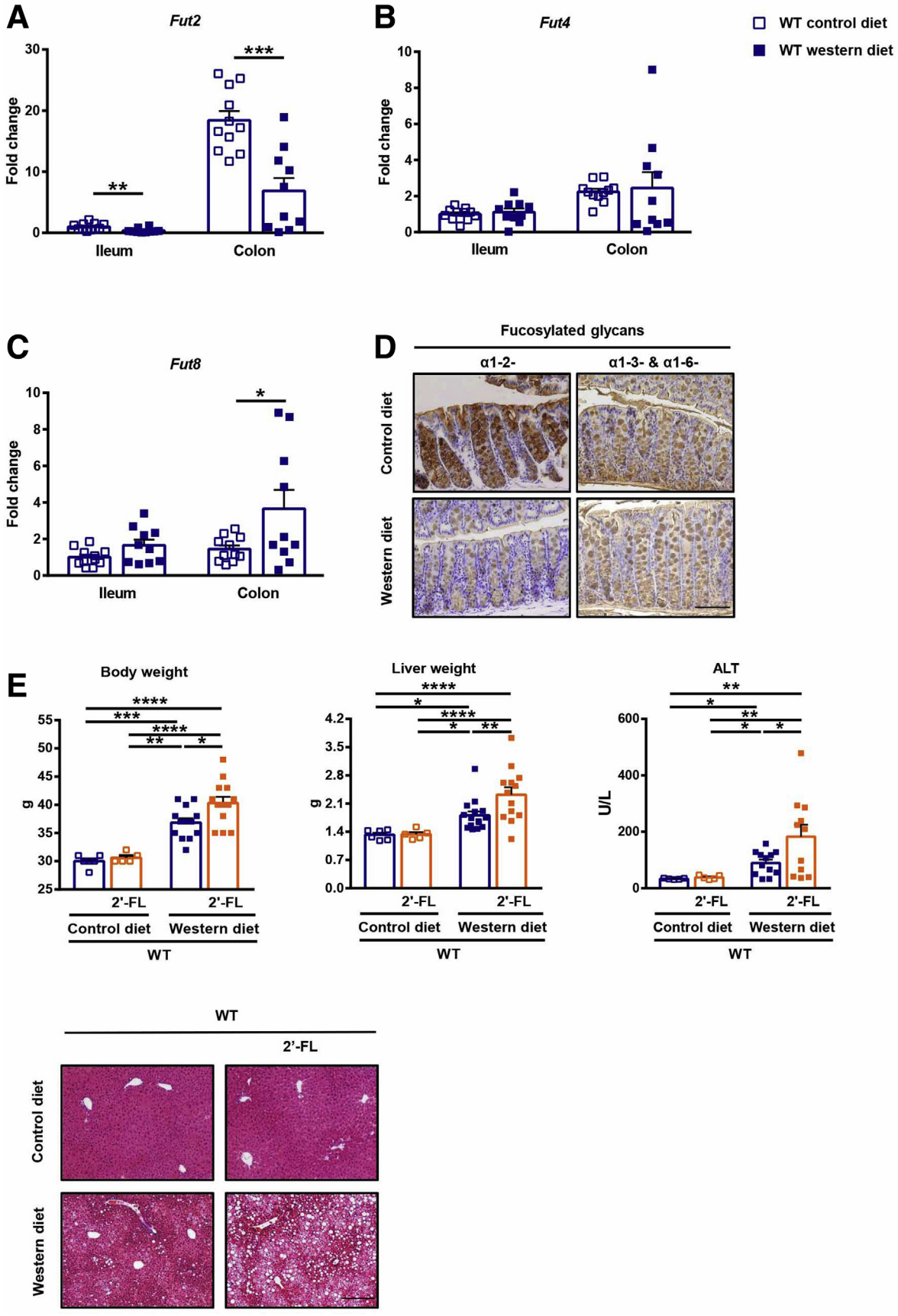
A
Fut2
Fold change
30
20
10
0
**
***
Ileum
Colon
B
Fut4
WT control diet
WT western diet
Fold change
10
8
6
4
2
0
Ileum
Colon
C
Fut8
Fold change
10
8
6
4
2
0
*
Ileum
Colon
D
Fucosylated glycans
α1-2-
α1-3- & α1-6-
Control diet
Western diet
E
Body weight
g
55
50
45
40
35
30
25
****
***
****
**
*
2'-FL
2'-FL
Control diet
Western diet
WT
Liver weight
g
4.2
3.5
2.8
2.1
1.4
0.7
0.0
****
*
****
*
**
2'-FL
2'-FL
Control diet
Western diet
WT
ALT
U/L
600
400
200
0
**
*
**
*
*
2'-FL
2'-FL
Control diet
Western diet
WT
WT
2'-FL
Control diet
Western diet

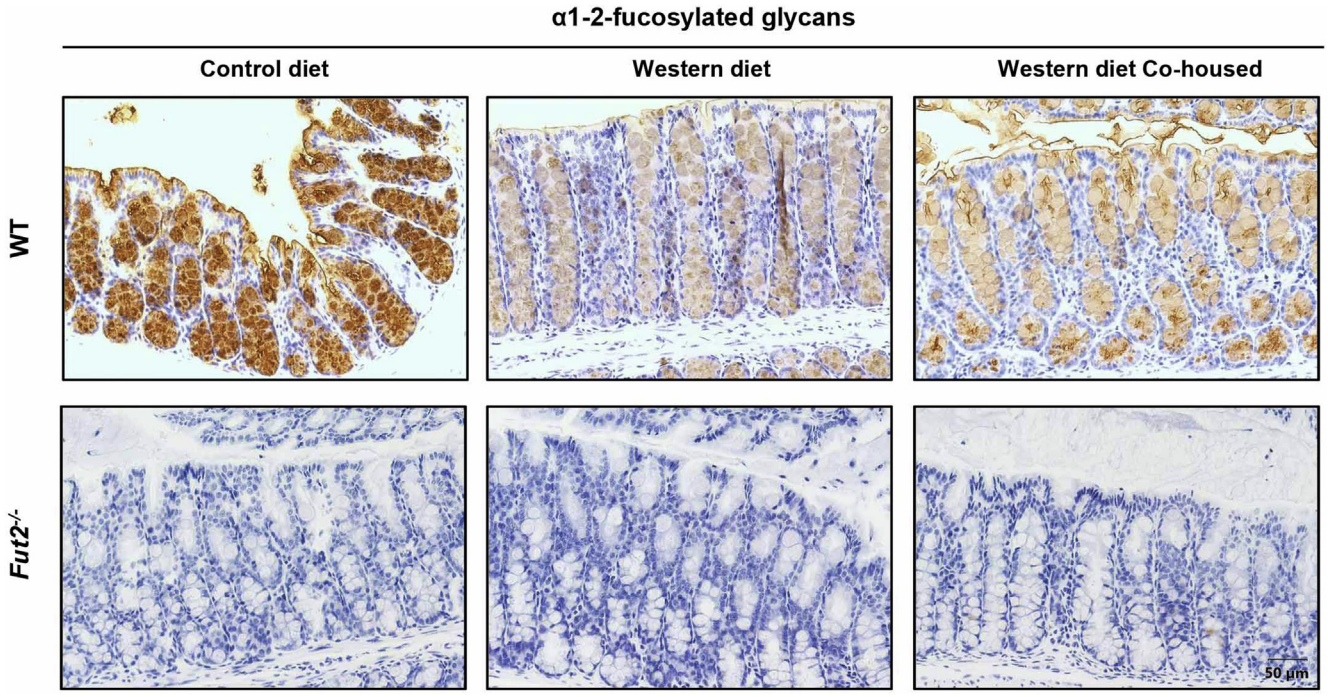

Figure 3. Intestinal α1-2-fucosylation in control and Western diet–fed mice. *Fut2*$^{-/-}$ and WT littermates were fed with either a control diet or a Western diet for 20 weeks. To facilitate fecal microbiota transfer we performed co-housing by feeding WT and *Fut2*$^{-/-}$ mice within 1 cage since weaning, and these mice were given a Western diet. Representative images of colon tissues with immunohistochemistry staining for α1-2-fucosylated glycans (with Ulex Europaeus Agglutinin I) are shown. Experiments were performed in n = 6 from 2–3 experiments.

diet–fed mice. In Western diet–fed mice, oxygen consumption (Vo_2) and carbon dioxide production (VCO_2) rate were slightly higher in *Fut2*$^{-/-}$ compared with WT mice (Figure 6*A*). Western diet–fed *Fut2*$^{-/-}$ mice had a higher respiratory exchange ratio, energy expenditure, and more vertical activity compared with WT mice (Figures 4*F* and 6*A*). These differences were more obvious during the dark cycles (Figure 6*A*) compared with the light cycles (Figure 6*B*), which is consistent with increased nocturnal activity of mice. In line with increased energy expenditure, Western diet–fed *Fut2*$^{-/-}$ mice generated more heat, with a significantly higher core body temperature (Figure 4*G*). An increased protein level of uncoupling protein 1 (Ucp1) in brown adipose tissue (Figure 4*H*) indicates augmented nonshivering thermogenesis in Western diet–fed *Fut2*$^{-/-}$ mice compared with WT mice. Taken together, *Fut2* deficiency increases energy expenditure and thermogenesis in brown adipose tissue, which might contribute to protection from Western diet–induced obesity.

Fut2 *Deficiency Attenuates Western Diet–Induced Steatohepatitis*

To assess the role of Fut2 for the development of steatohepatitis, we investigated parameters of liver injury, steatosis, inflammation, and fibrosis. Western diet–induced liver injury as assessed by levels of ALT (Figure 7*A*) and hepatic steatosis as evaluated by liver weight, hepatic triglycerides, and H&E staining (Figure 7*B* and *C*) were lower in Western diet–fed *Fut2*$^{-/-}$ mice compared with WT mice. Hepatic expression of inflammatory genes such as *Tnfα* and *Ccl2* (Figure 7*D*), and genes related to fibrosis such as *Acta2*

Figure 2. (***See previous page***). **Western diet feeding reduces intestinal α1-2-fucosylation in mice.** WT C57BL/6 mice were fed with either control diet and regular water (control diet groups) or Western diet combined with glucose (18.9 g/L) and fructose (23.1 g/L) in drinking water (Western diet groups) for 20 weeks. (*A*) Expression of *Fut2* mRNA in ileum and colon tissue. (*B*) Expression of *Fut4* mRNA in ileum and colon tissue. (*C*) Expression of *Fut8* mRNA in ileum and colon tissue. (*D*) Representative images of colon tissues with immunohistochemistry staining for α1-2–linked (with Ulex Europaeus Agglutinin I), α1-3–linked (with Aleuria Aurantia Lectin), and α1-6–linked (with Aleuria Aurantia Lectin) fucosylation. WT mice were assigned to the 2'-FL–treated group and control group, and fed with either a control diet or a Western diet. In the 2'-FL–treated group, 2'-FL (2 g/L) was supplemented continuously in drinking water. The experimental diet and 2'-FL treatment lasted for 20 weeks. (*E*) Body weight, liver weight, plasma ALT levels, and representative images of H&E-stained liver tissue. *Scale bar*: 200 μm. Gene expression data are relative to ileum of control diet mice and all the data are presented as means ± SEM. **P* < .05, ***P* < .01, ****P* < .001, and *****P* < .0001. *(A-C)* The Student unpaired *t* test was used. *(E)* One-way analysis of variance followed by the Tukey post hoc test was used for comparison between groups. (*A–D*) Experiments performed in n = 11 on a control diet and n = 10 on a Western diet from 2–3 experiments, and for (*E*) experiments performed in n = 5–6 on a control diet and n = 10–14 on a Western diet from 2–3 experiments.

and *Tgfb1* (Figure 7*E*) were lower in *Fut2*$^{-/-}$ mice compared with WT mice following a Western diet for 20 weeks. Sirius red staining further showed the protective effect of *Fut2* deficiency against Western diet–induced liver fibrosis (Figure 7*F*). Calorie-restricted and Western diet–fed *Fut2*$^{-/-}$ mice were fully protected from steatohepatitis as indicated by similar levels of ALT, steatosis, inflammation, and fibrosis parameters compared with control diet–fed groups (Figure 7). These findings indicate that *Fut2* deficiency attenuates Western diet–induced steatohepatitis.

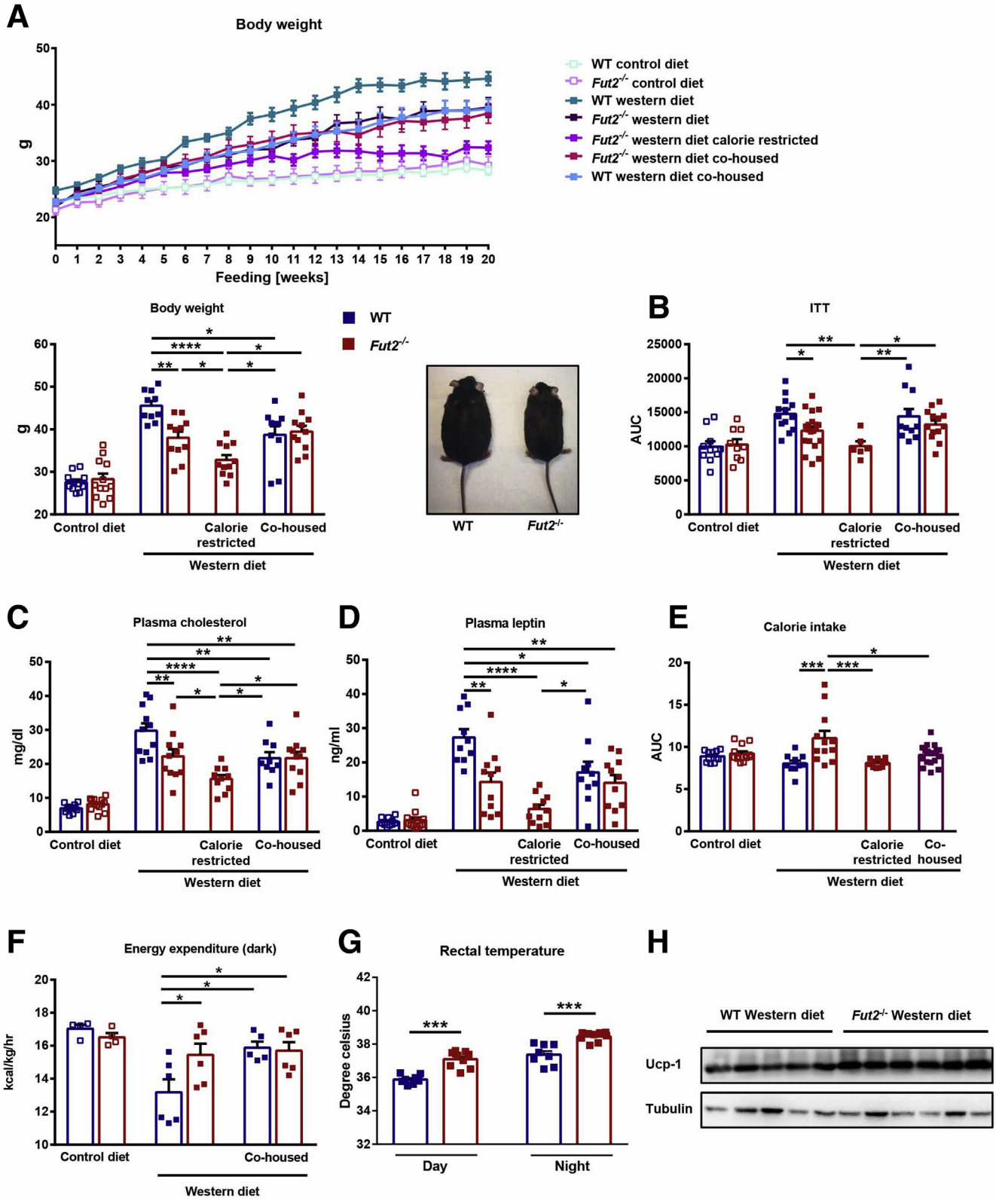

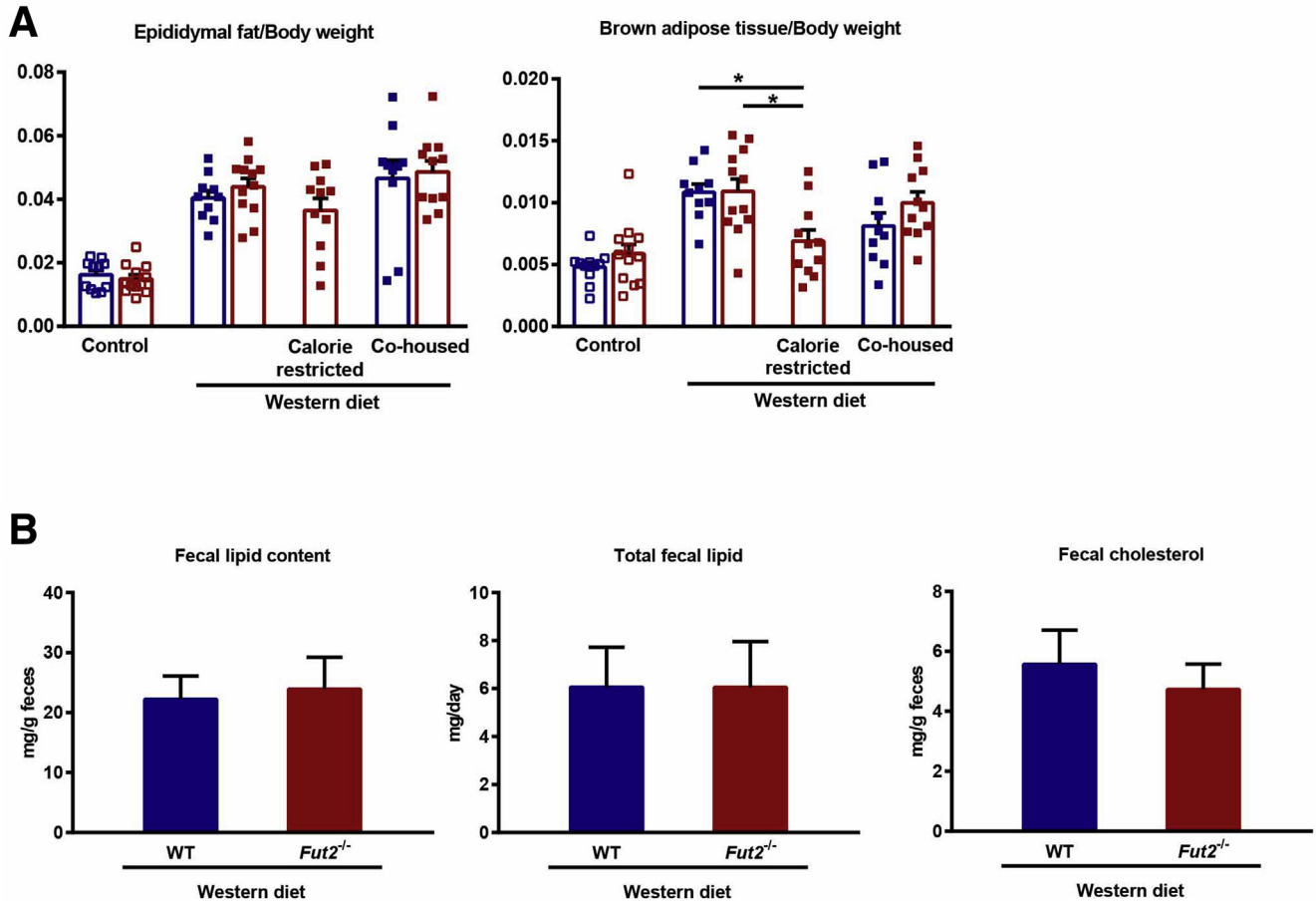

Figure 5. Adipose tissue and fecal lipids in Western diet–fed mice. *Fut2*$^{-/-}$ and WT littermates were fed with either a control diet or a Western diet for 20 weeks. Western diet–fed *Fut2*$^{-/-}$ mice had a significantly higher caloric intake than WT littermate mice. The total caloric intake of *Fut2*$^{-/-}$ mice was restricted to make it equal to the caloric intake of WT mice during Western diet feeding (calorie-restricted group). (*A*) Weight of epididymal white adipose tissue and brown adipose tissue normalized to body weight. (*B*) Fecal lipid content. Data represent means ± SEM. *$P < .05$. (*A*) One-way analysis of variance followed by the Tukey post hoc test was used for comparison between Western diet groups. (*B*) The Student unpaired *t* test was used. Experiments were performed in n = 5–13 per group from 3–5 experiments.

Protection From Obesity and Steatohepatitis Associated With Fut2 *Deficiency Is Transmissible via Microbiota Exchange and Reduced by Antibiotic Treatment*

Because intestinal α1-2-fucosylation is important for regulating the intestinal microbiota,[16,18] we performed co-housing studies. Co-housing of mice in the same cage results in fecal microbiota transfer between mice. Strikingly, co-housing of WT littermates and *Fut2*$^{-/-}$ mice conferred protection from features of Western diet–induced obesity and steatohepatitis to WT mice (Figures 4*A–E*, 6*A-B*, 7*A-F*), indicating that the phenotype is transmissible via fecal microbiota transfer. Spots of α1-2-fucosylated glycans were

Figure 4. (***See previous page***). ***Fut2* deficiency protects mice from diet-induced obesity.** *Fut2*$^{-/-}$ and WT littermates were fed with either a control diet or a Western diet for 20 weeks. Western diet–fed *Fut2*$^{-/-}$ mice had a significantly higher caloric intake than WT littermate mice and we restricted the total caloric intake of *Fut2*$^{-/-}$ mice to make it equal to the caloric intake of WT mice during Western diet feeding (calorie-restricted group). To facilitate fecal microbiota transfer between mice, freshly weaned WT and *Fut2*$^{-/-}$ mice were co-housed in the same cage and subjected to Western diet feeding. (*A*) Body weight and representative images for WT and *Fut2*$^{-/-}$ Western diet–fed mice. (*B*) Insulin tolerance test (ITT) was performed after 19 weeks of control or Western diet feeding. (*C*) Plasma cholesterol levels. (*D*) Plasma leptin levels. (*E*) Area under curve (AUC) of calorie intake over the course of the experiment. After 20 weeks of control or Western diet feeding, mice were housed in the comprehensive laboratory animal monitoring system metabolic cages for the measurement of metabolic data. (*F*) Energy expenditure was calculated by Vo_2 and respiratory exchange ratio (RER). (*G*) Rectal temperatures at room temperature. (*H*) Immunoblot for Ucp1 in brown adipose tissue. Data represent means ± SEM. *$P < .05$, **$P < .01$, ***$P < .001$, and ****$P < .0001$. One-way analysis of variance followed by the Tukey post hoc test was used for comparison between Western diet groups. Experiments were performed in n = 5–13 per group from 3–5 experiments. For the insulin tolerance test n = 13 in the WT Western diet group and n = 20 in the *Fut2*$^{-/-}$ Western diet group from 5 experiments. For the metabolic cages, n = 4–6 per group from 3 experiments.

observed in the intestine of *Fut2*$^{-/-}$ co-housed mice (likely owing to α1-2-fucosylated glycans from feces in coprophagic mice), but completely absent in control and Western diet–fed *Fut2*$^{-/-}$ mice. Co-housed and Western diet–fed WT mice showed lower expression of α1-2-fucosylated glycans compared with WT mice fed a control diet, but this was similar to Western diet–fed WT mice (Figure 3). Our co-housing studies indicate that the phenotype is transmissible via fecal microbiota transfer.

To further show a contribution of the intestinal microbiota, gut bacteria were reduced with antibiotics.[20,21] WT and *Fut2*$^{-/-}$ mice on a Western diet for 12–13 weeks received antibiotics for an additional 5 weeks, while being continued on a Western diet. Antibiotic-treated *Fut2*$^{-/-}$ Western diet–fed mice were no longer protected from obesity and steatohepatitis compared with vehicle-treated *Fut2*$^{-/-}$ mice because they gained more body weight and had more severe liver disease (Figure 8). Ucp1 protein expression in brown adipose tissue did not change in antibiotic-treated *Fut2*$^{-/-}$ mice compared with vehicle-treated *Fut2*$^{-/-}$ mice following Western diet feeding (data not shown). On the contrary, WT Western diet–fed mice treated with antibiotics lost body weight and showed improved steatohepatitis compared with vehicle-treated WT mice (Figure 8), which could be the result of a decrease in systemic lipopolysaccharide levels after antibiotic treatment as reported.[21,22] We found a trend toward decreased *Fut2* mRNA in the colon of Western diet–fed WT mice treated with antibiotics compared with vehicle-treated Western diet–fed WT mice (Figure 8*D*), which could contribute to lower body weight in antibiotic-treated WT mice. These findings further support an important role of the intestinal microbiota mediating the effect of *Fut2* deficiency in protecting from diet-induced obesity and steatohepatitis.

Fut2-*Deficient Mice Show an Altered Plasma Metabolome and Intestinal Microbiome*

One possible mechanism for the protection from obesity and steatohepatitis of co-housed WT mice could be through transfer of beneficial intestinal metabolites and/or microbes associated with *Fut2* deficiency. We therefore combined plasma metabolomics with fecal metagenomics. WT and *Fut2*$^{-/-}$ Western diet–fed mice showed different plasma metabolomic profiles (Figure 9*A*). One of the most prominent changes in plasma metabolites was found with bile acids. Total plasma bile acids not only were decreased significantly in Western diet–fed *Fut2*$^{-/-}$ mice compared with Western diet–fed WT mice (Figure 10*A*), but *Fut2*$^{-/-}$ mice had higher proportions of secondary and lower proportions of primary bile acids in plasma and the large intestine (cecum) than WT mice after feeding a Western diet (Figure 10*B* and *C*). The majority of bile acids were primary bile acids, and the proportions between primary and secondary bile acids were not different in the proximal and mid-small intestine (duodenum and jejunum) between WT and *Fut2*$^{-/-}$ Western diet–fed mice (Figure 11*A*), which indicates an important role of bile acid–metabolizing bacteria in the distal small and large intestine. Co-housed WT mice also showed a trend toward a higher proportion of secondary and lower proportion of primary bile acids in the cecum and plasma (Figure 10*B* and *C*). At baseline, WT and *Fut2*$^{-/-}$ mice not only had similar levels of plasma bile acids (Figure 10*A*), but also a similar composition of plasma and cecum bile acids (Figure 11*B* and *C*).

To evaluate the taxonomic composition and microbial diversity, shotgun metagenomic libraries of mouse fecal samples were sequenced and co-assembled to generate nearly complete genomes. Taxonomic analysis showed similar changes between WT and *Fut2*$^{-/-}$ mice in bacterial composition (Figure 9*B*) and diversity after Western diet feeding (Figure 9*C*). Functional analysis using mouse catalog genes[23] showed that the relative abundance of bacterial enzyme 7-α-hydroxysteroid dehydrogenases (7α-HSDH, encoded by the *hsdh* gene) participated in the conversion of primary into secondary bile acids,[24–28] and was increased significantly in Western diet–fed *Fut2*$^{-/-}$ mice compared with Western diet–fed WT mice (Figure 10*D*). The relative abundance of the *hsdh* gene showed the same trend of increase in co-housed WT and *Fut2*$^{-/-}$ groups compared with WT mice on a Western diet (Figure 10*D*).

Taken together, *Fut2*$^{-/-}$ mice had a higher relative abundance of the bacterial enzyme 7α-HSDH, which is an important and broadly distributed enzyme in converting primary into secondary bile acids, and this might explain the different patterns of plasma and intestinal bile acids after Western diet feeding.

Fut2 *Deficiency Attenuates Western Diet–Induced Dysregulation of Bile Acid Metabolism*

To further study the impact of *Fut2*$^{-/-}$ deficiency on bile acid metabolism, we measured bile acids in different compartments. Consistent with lower plasma bile acids, Western diet–fed *Fut2*$^{-/-}$ mice showed lower total bile acids in the liver and a decreased bile acid pool size compared with Western diet–fed WT mice (Figure 12*A*). A decrease in the bile acid pool can be caused by reduced bile acid synthesis and/or by an increase in bile acid excretion. Indeed, we found that feces of *Fut2*$^{-/-}$ mice contained more bile acids than feces of WT mice after a Western diet (Figure 12*B*). *Slc10a2* (also called apical *Na*$^{+}$*-dependent bile salt transporter*), which is responsible for the uptake of primary bile acids in the terminal ileum, was expressed similarly in all mouse groups (Figure 12*C*). These results indicate that an increased intestinal conversion of primary into secondary bile acids with a subsequent lower reuptake of secondary bile acids likely is responsible for increased fecal bile acid excretion.

In addition, *Fut2*$^{-/-}$ mice showed a decrease of cytochrome P450, family 7, subfamily a, polypeptide 1 (Cyp7a1) protein (Figure 12*F*), but increased cholesterol in the liver (Figure 12*D*) compared with WT mice after a Western diet, indicating that bile acid synthesis from cholesterol is lower in *Fut2*$^{-/-}$ mice. Hepatic cytochrome P450, family 8, subfamily b, polypeptide 1 (*Cyp8b1*) mRNA expression was not significantly different between mouse groups (Figure 12*E*).

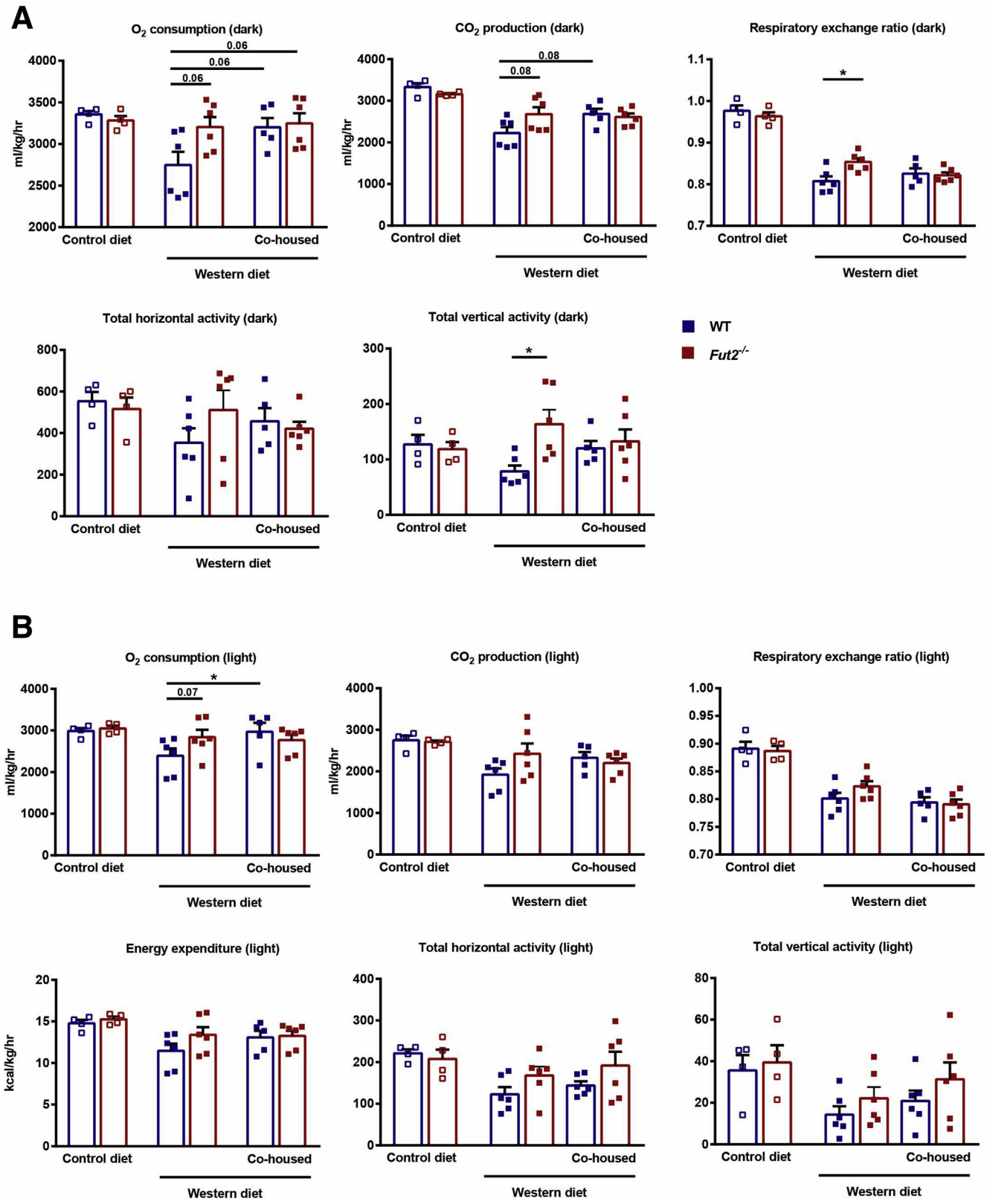

Figure 6. Western diet–fed *Fut2*-deficient mice have increased energy expenditure. *Fut2*$^{-/-}$ and WT littermates (normal groups and co-housed groups) were fed with either a control diet or a Western diet for 20 weeks. After 20 weeks of feeding mice were housed in the comprehensive laboratory animal monitoring system metabolic cages for the measurement of metabolic data, including Vo_2, VCO_2, respiratory exchange ratio, rate of energy expenditure calculated by VO_2 and respiratory exchange ratio, and cumulative ambulatory counts for horizontal and vertical activity. (*A*) Metabolic parameters in dark cycles. (*B*) Metabolic parameters in light cycles. Data represent means ± SEM. *$P < .05$. One-way analysis of variance followed by the 2-stage step-up method of Benjamini, Krieger, and Yekutieli test was used for comparison between Western diet groups. Experiments were performed in n = 4–6 per group from 3 experiments.

Farnesoid X receptor (FXR, encoded by the *Nr1h4* gene)–induced expression of fibroblast growth factor (Fgf)15 in the terminal ileum is known to suppress Cyp7a1 in the liver. Expression of intestinal *Nr1h4* and *Fgf15* mRNA was up-regulated in all Western diet–fed mice, but Western diet–fed WT mice had the highest levels (Figure 12*G*). Despite increased *Fgf15*, Western diet–fed WT mice had the highest Cyp7a1 protein levels (Figure 12*F*), indicating that the negative feedback regulation of bile acid synthesis is nonfunctional. Cyp7a1 is regulated additionally by hepatic

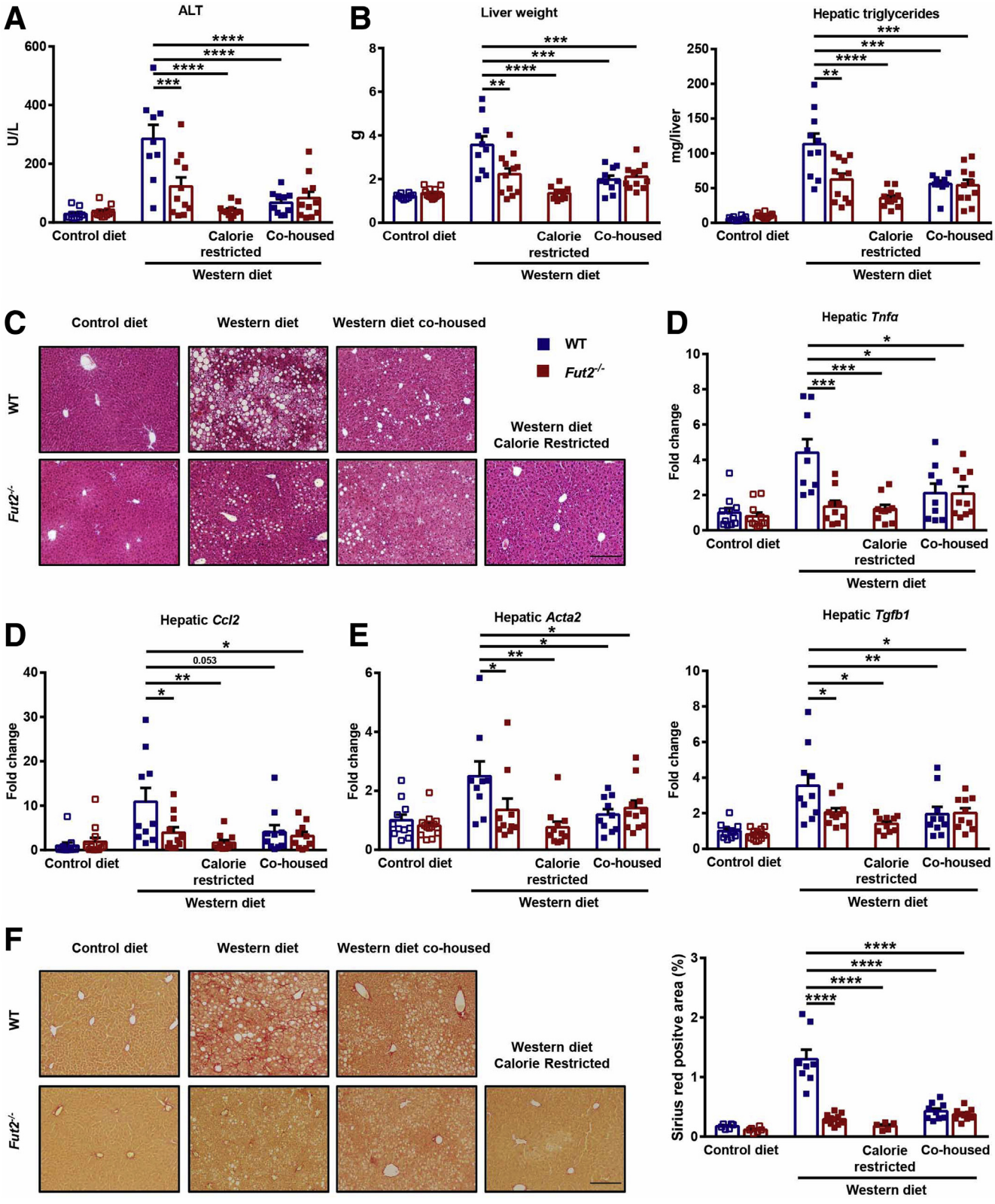

FXR. We therefore measured systemic FXR activity using a reporter assay. FXR activity was significantly higher in Western diet–fed WT mice than in *Fut2*$^{-/-}$ mice and control diet mice (Figure 12*H*). Changes that we have observed in *Fut2*$^{-/-}$ mice were similar in calorie-restricted *Fut2*$^{-/-}$ mice and co-housing groups, confirming the transmissibility of the phenotype (Figure 12*A*–*G*). These findings indicate that despite increased total bile acids, WT mice are not able to down-regulate bile acid synthesis and appear to be resistant to increased Fgf15 and higher systemic FXR activity. In contrast, changes in intestinal bile acid metabolism associated with *Fut2* deficiency results in increased fecal bile acid secretion, decreased bile acid synthesis, and a lower bile acid pool.

Supplementation of Exogenous α1-2-Fucosylated Glycans Exacerbates Steatohepatitis

To test whether we can overcome genetic *Fut2* deficiency by dietary supplementation of α1-2-fucosylated glycans, *Fut2*$^{-/-}$ mice were administered 2′-FL together with a Western diet or control diet. *Fut2*$^{-/-}$ mice supplemented with 2′-FL gained significantly more body and liver weight (Figure 13*A* and *B*), and had a similar caloric intake as *Fut2*$^{-/-}$ mice fed a Western diet alone (Figure 14*A*). Western diet–fed *Fut2*$^{-/-}$ mice supplemented with 2′-FL showed increased liver injury (Figure 13*C*), higher plasma bile acids, a higher proportion of plasma primary bile acids and a lower proportion of plasma secondary bile acids (Figure 14*B*), increased hepatic steatosis (Figure 13*D*), and a higher expression of inflammatory and fibrosis-related genes, including *Tnfα*, *Ccl2*, and *Col1a1* (Figure 14*C*) compared with *Fut2*$^{-/-}$ mice not receiving 2′-FL. Supplementation with 2′-FL caused a significant decrease in the proportion of deoxycholic acid (DCA) and lithocholic acid in plasma (Figure 14*D*), which are secondary bile acids generated by the enzyme 7α-HSDH,[29–31] supportive of lower enzyme activity of 7α-HSDH under this condition. Consistent with results in chow diet–fed WT mice (Figure 2*E*), 2′-FL supplementation did not increase features of the metabolic syndrome including body weight gain and steatohepatitis in chow-fed *Fut2*$^{-/-}$ mice (Figure 13).

To determine whether L-fucose itself exerts any metabolic effects, WT mice were administered L-fucose together with the Western diet. Consistent with a previous report,[32] Western diet–fed WT mice supplemented with L-fucose gained less body weight (Figure 15*A*). Western diet–fed WT mice supplemented with or without L-fucose had similar caloric intake (Figure 15*B*). Western diet–fed WT mice supplemented with L-fucose showed lower ALT levels (Figure 15*C*), lower liver weight (Figure 15*D*), and reduced hepatic steatosis as evidenced by hepatic triglycerides and H&E staining (Figure 15*E*). These findings indicate that α1-2-linked fucose but not L-fucose alone is responsible for the obesity and steatohepatitis-promoting effect.

Discussion

Epithelial α1-2-fucosylation is induced once commensal bacteria colonize the gut and is observed predominantly in the ileum and colon.[14] In this study, we observed decreased intestinal α1-2-fucosylation in Western diet–fed mice, and restoration of intestinal α1-2-fucosylation with orally administered α1-2-fucosylated glycans exacerbated obesity and steatohepatitis. On the contrary, *Fut2* deficiency attenuated diet-induced obesity and steatohepatitis despite a higher caloric intake than WT mice. Remarkably, protection from this phenotype (rather than the disease) is transmissible via fecal microbiota transfer and depletion of the gut microbiota by antibiotic treatment reduced differences between Western diet–fed WT and *Fut2*-deficient mice. Oral supplementation of α1-2-fucosylated glycans in the form of 2′-FL offsets the protective effect of *Fut2* deficiency against features of the metabolic syndrome. We have linked *Fut2* deficiency with changes in the microbial metabolism of bile acids. These data suggest a critical role of intestinal α1-2-fucosylation for the pathogenesis of obesity and steatohepatitis.

Fut2 polymorphism is associated with various disease conditions in human beings. Approximately 20% of Caucasians have nonfunctional variants of *Fut2* on both alleles (also called *nonsecretor phenotype*), which is caused mainly by the single-nucleotide polymorphism rs601338.[33] Secretor individuals have functional *Fut2* alleles (genotype GG).[34] Therefore, secretors can produce α1-2-fucosylated components, while nonsecretors lack this activity. Nonsecretor status increases susceptibility to primary sclerosing cholangitis (PSC) and Crohn's disease.[35,36] Lack of intestinal fucosylation results in altered intestinal microbiota, gut barrier function, and pathogen adhesion under disease conditions.[18,37–42] For instance, in a chemical-induced colitis mouse model, Fut2-mediated intestinal α1-2-fucosylation protects against intestinal pathobionts such as *Enterococcus faecalis* and *Citrobacter rodentium* infection.[18] In our

Figure 7. (***See previous page***). ***Fut2* deficiency attenuates diet-induced steatohepatitis in mice.** *Fut2*$^{-/-}$ and WT littermates were fed with either a control diet or a Western diet for 20 weeks. Western diet–fed *Fut2*$^{-/-}$ mice had a significantly higher caloric intake than WT littermate mice and we restricted the total caloric intake of *Fut2*$^{-/-}$ mice to make it equal to the caloric intake of WT mice during Western diet feeding (calorie-restricted group). To facilitate fecal microbiota transfer between mice, freshly weaned WT and *Fut2*$^{-/-}$ mice were co-housed in the same cage and subjected to Western diet feeding. (*A*) Plasma ALT levels. (*B*) Liver weight and hepatic triglyceride levels. (*C*) Representative images of H&E-stained liver tissue. (*D*) Hepatic *Tnfα* and *Ccl2* mRNA levels. (*E*) Hepatic *Acta2* and *Tgfb1* mRNA levels. (*F*) Representative images of Sirius red–stained liver tissue, and Sirius red–positive area was quantitated by image analysis software. Data represent means ± SEM. **P* < .05, ***P* < .01, ****P* < .001, and *****P* < .0001. One-way analysis of variance followed by the Tukey post hoc test was used for comparison between Western diet groups. *Scale bars*: 200 μm. Experiments were performed in n = 10–13 per group from 3–5 experiments. For the H&E and Sirius red staining, n = 5–6 in control diet groups and n = 8–11 in Western diet groups from 2 experiments.

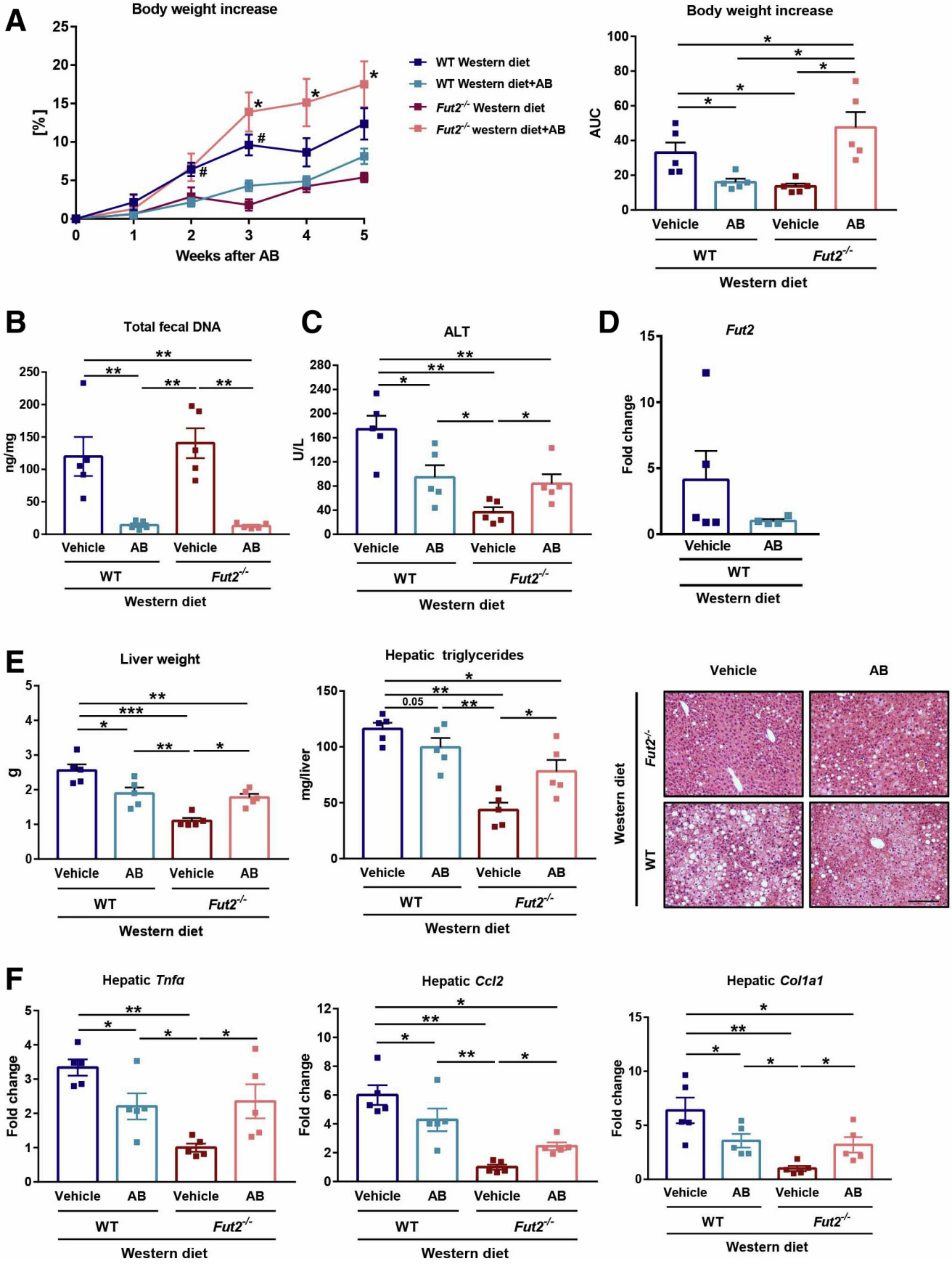
A
Body weight increase
[%]
Weeks after AB
WT Western diet
WT Western diet+AB
Fut2-/- Western diet
Fut2-/- western diet+AB
Body weight increase
AUC
Vehicle
AB
Vehicle
AB
WT
Fut2-/-
Western diet
B
Total fecal DNA
ng/mg
C
ALT
U/L
D
Fut2
Fold change
E
Liver weight
g
Hepatic triglycerides
mg/liver
Vehicle
AB
Western diet
F
Hepatic Tnfα
Hepatic Ccl2
Hepatic Col1a1
Fold change

study, *Fut2*$^{-/-}$ mice (mimicking the nonsecretor status) were no longer protected from Western diet–induced obesity and steatohepatitis when α1-2-fucosylated glycans were restored in the intestine after oral administration of 2'-FL. Dietary supplementation of α1-2-fucosylated glycans (mimics transgenic overexpression of *Fut2*) not only abrogates the protective effects of genetic *Fut2* deficiency, but also exacerbates the disease in Western diet–fed WT mice. Based on these findings, the down-regulation of intestinal α1,2-fucosylation in WT mice might be a defense mechanism against the harmful effects of a Western diet, and likely is regulated by changes in gut bacteria and the host's response to a Western diet. Although 2'-FL is only known to be present in human milk, 2'-FL currently is used as a supplement to infant formula with claims to benefit infant growth. However, long-term effects of early life exposure to 2'-FL, especially in nonsecretor infants, remain unknown. Large patient population studies are needed to clarify the impact of Fut2 polymorphism on human obesity and NASH pathogenesis. Simple genome-wide association studies might be confounded by a functional down-regulation in Fut2 activity after eating a Western diet.

The limitation of our study was the use of a whole-body *Fut2* knockout mouse, which cannot exclude the effect of *Fut2* deficiency in organs other than the intestine. In addition to the distal small intestine, Fut2 is highly expressed in gallbladder epithelial cells, but not in liver bile duct cells. A possible effect of Fut2 deficiency in gallbladder epithelial cells on bile acid metabolism should be considered. In *Fut2* nonsecretor individuals the absence of α-1,2-fucosylated glycans was associated with higher disease progression and increased risk of biliary *Candida* infections in patients with PSC.[43] Human hydrophobic bile acids induce more hepatobiliary damage in *Fut2* knockout mice than WT mice.[44] However, the role of *Fut2* deficiency in all of these studies was associated with more biliary and liver disease, which is the opposite we found in our diet-induced obesity and steatohepatitis model. It is possible that the potential disadvantages of Fut2 deficiency for the hepatobiliary system is compensated by beneficial microbiota-mediated effects such as modulation of bile acids. To some extent, the whole-gene knockout mouse is closer to the physiological situation of a human nonsecretor status, but future studies with a tissue-specific deletion of Fut2 in intestinal epithelial cells are required.

Alterations of intestinal microbiota are involved in the pathogenesis of obesity and NASH.[45,46] Bile acids are modified by the intestinal microbiota and act on both hepatic and extrahepatic tissues to maintain energy homeostasis through regulation of lipid and carbohydrate metabolic pathways.[47] Thus, bile acids are the most promising signaling molecules that link obesity and NASH to intestinal microbiota. Increased serum bile acids are observed in patients with NASH, and excessive accumulation of bile acids in the liver induces hepatocyte death, inflammation, and progressive liver damage.[48,49] Although 1 study reported that half of *Fut2*$^{-/-}$ mice had 40 times higher serum bile acids levels compared with WT mice,[44] this was not identified in our study. *Fut2*$^{-/-}$ mice have similar plasma bile acids levels and bile acid components compared with WT littermate mice at baseline. After Western diet feeding, mice had increased liver cholesterol and this enhances the synthesis of bile acids by up-regulation of Cyp7a1. Biliary secretion of bile acids into the intestine and its reabsorption will be increased, resulting in an enlargement of the bile acid pool size. Provided that the negative feedback mechanism through intestinal FXR/Fgf15 is functioning properly—as we observed in our Western diet–fed *Fut2*$^{-/-}$ mice—increased intestinal bile acids will activate intestinal FXR, suppress Cyp7a1, and eventually decrease bile acid synthesis. In addition to this mechanism to reduce the bile acid pool, Western diet–fed *Fut2*$^{-/-}$ mice had increased fecal excretion of bile acids, likely owing to compositional changes and a higher proportion of secondary bile acids in the intestine. Functional metagenomic analysis showed a higher abundance of the bacterial gene encoding the enzyme 7α-HSDH in Western diet–fed *Fut2*$^{-/-}$ mice. 7α-HSDH is widely distributed in intestinal bacteria, including but not limited to *Bacteroides*, *Clostridia*, *Escherichia coli*, and *Ruminococcus* species, and participates in the oxidation and dehydroxylation of bile acids.[24,25,28] Therefore, changes in primary and secondary bile acids in WT and *Fut2*$^{-/-}$ Western diet–fed mice might not be owing to a single bacterium, but rather caused by a bacterial community. Reduction of the bacterial *hsdh* gene has been reported in type 2 diabetes mellitus patients.[50] Unlike Western diet–fed *Fut2*$^{-/-}$ mice, NASH patients have increased primary (mainly cholic acid and chenodeoxycholic acid) and decreased secondary (mainly deoxycholic acid and lithocholic acid) plasma bile acids; a higher ratio of total secondary bile acid to primary bile acid decreases the likelihood of significant fibrosis.[51] NASH and NAFLD patients also have an increased primary to secondary ratio of fecal bile acids.[49] In summary, changes in the intestinal microbiota associated with Western diet–fed *Fut2*$^{-/-}$ mice

Figure 8. (***See previous page***). **Protection from obesity and steatohepatitis associated with *Fut2* deficiency is reduced by antibiotic treatment.** WT and *Fut2*$^{-/-}$ mice fed a Western diet for 12–13 weeks were gavaged with antibiotics for 5 weeks to reduce gut microbiota. Control vehicle mice were gavaged with the same amount of sterile water. (*A*) Body weight changes and area under the curve of body weight increase during the course of the antibiotic treatment. (*B*) Total fecal DNA amount. (*C*) Plasma ALT levels. (*D*) Colon *Fut2* mRNA level in WT mice. (*E*) Liver weight, hepatic triglyceride levels, and representative images of H&E-stained liver tissue. (*F*) Hepatic *Tnf*α, *Ccl2*, and *Col1a1* mRNA levels. Data represent means ± SEM. **P* < .05, ***P* < .01, and ****P* < .001. (*A*) **P* < .05 compared with *Fut2*$^{-/-}$ Western diet group; $^{\#}$*P* < .05 compared with WT Western diet antibiotic group. One-way analysis of variance followed by the 2-stage step-up method of Benjamini, Krieger, and Yekutieli test was used. *Scale bar*: 200 μm. Experiments were performed in n = 5 per group from 2 experiments. AB, antibiotic treatment.

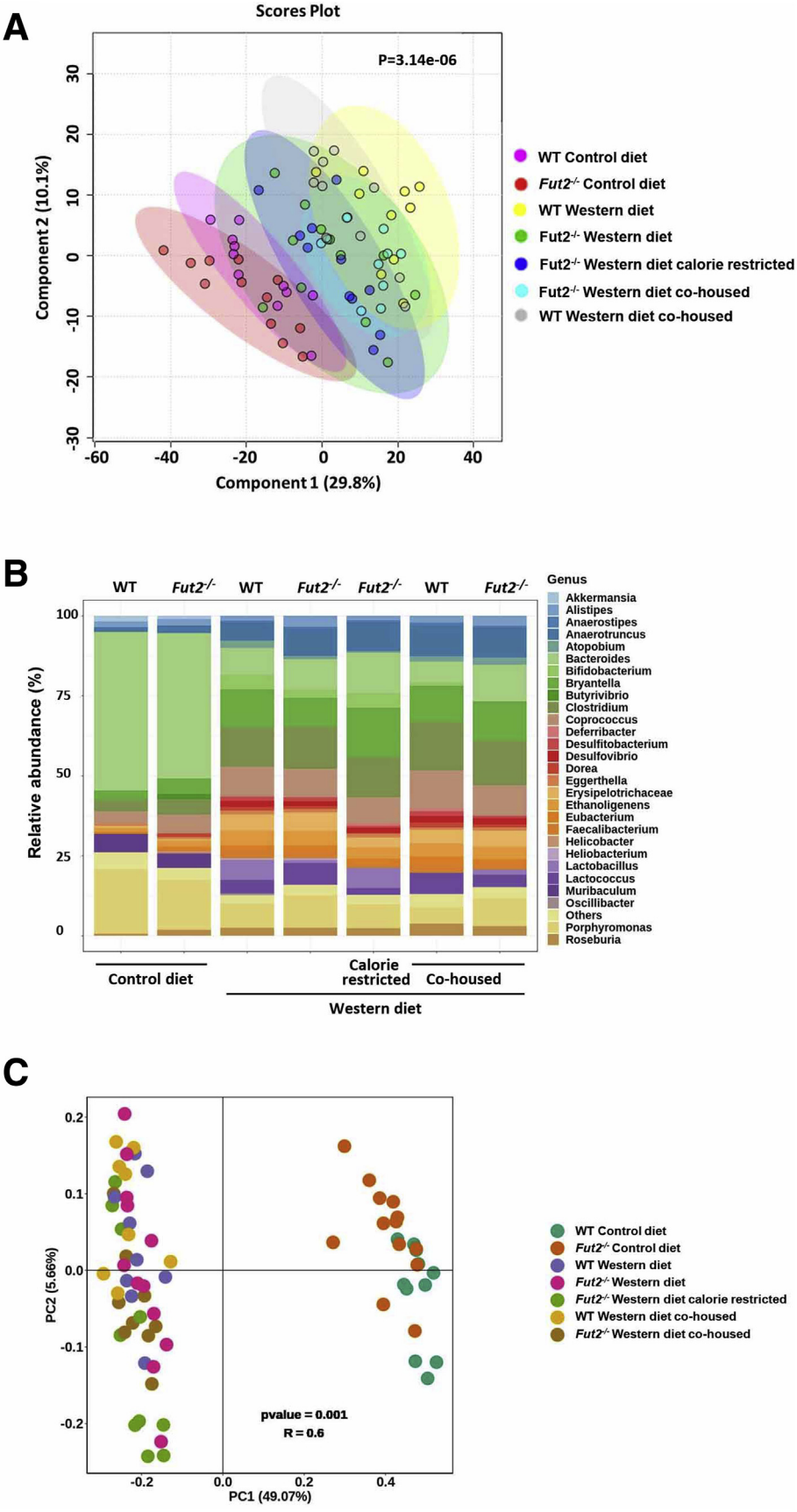

Figure 9. *Fut2* deficiency mice have altered plasma metabolome and intestinal microbiota. *Fut2*$^{-/-}$ and WT littermates were fed with either a control diet or a Western diet for 20 weeks. (*A*) There were 1984 different plasma metabolites quantified by untargeted metabolomics, and principal component analysis and hierarchical cluttering of metabolomics data were performed using MetaboAnalyst 4.0. (*B, C*) Genomic DNA from mouse feces was extracted and purified for shotgun metagenomic sequencing. Rarefied reads from 73 samples were combined and assembled to generate near-complete genomes. The genomes were used to evaluate taxonomy and microbial diversity among the 7 groups. (*B*) Relative abundance of intestinal bacteria at genus level. (*C*) The β diversity of intestinal microbiota was analyzed by principal coordinate analysis. Experiments were performed in n = 10–13 per group from 3 experiments. PC, principal coordinate.

result in a decreased bile acid pool size by activating intestinal FXR signaling pathways and increasing fecal excretion of bile acids. This will prevent excessive accumulation of bile acids and liver damage.

The negative feedback mechanism through FXR/Fgf15 inhibits transcription of Cyp7a1 in hepatocytes and limits de novo synthesis of bile acids.[52] Western diet–fed WT mice had a higher level of taurocholic acid (TCA) in the plasma (data not shown), which can act as an agonist of FXR and might contribute to increased serum FXR activity in these mice. However, the activation of FXR failed to inhibit bile acid synthesis in our Western diet–fed WT mice. Several studies have reported similar findings of increased FXR activation and increased bile acid synthesis in NAFLD/NASH patients and animal models.[53–56] For instance, after an oral fat challenge, NAFLD patients without insulin resistance had an increase of plasma Fgf19 accompanied by a lower plasma level of the de novo bile acid synthesis marker C4 (7α-hydroxy-4-cholesten-3-one), while NAFLD patients with insulin resistance who had increased plasma Fgf19, a decrease of C4 was not observed. The most likely mechanism is that NAFLD/NASH patients had an impaired hepatic response to Fgf19 leading to dysregulation of bile acid synthesis and an increased total bile acid pool.[53–56] GW4064 is a classic FXR agonist and was shown to be effective in repressing bile acid synthesis and hepatic steatosis in several previous studies. However, in our WT Western diet mice, GW4064 treatment failed to decrease bile synthesis and was not able to reduce obesity and hepatic steatosis (data not shown), this further supports that these mice were resistant to FXR/Fgf15 activation. The mechanism that causes nonresponse of Cyp7a1 to FXR activation is poorly understood. Increased plasma free fatty acids[54] and hepatic microRNA-34a[55] can prevent FXR-mediated repression of Cyp7a1 expression, however, further studies are needed to elucidate the mechanism of this resistance.

Western diet–fed *Fut2*$^{-/-}$ mice had a higher energy expenditure and an increase of nonshivering thermogenesis in brown adipose tissue indicated by a higher core body temperature and UCP-1 protein expression in brown adipose tissue than WT mice, and this is likely the main reason for the protection from diet-induced obesity and hepatic steatosis despite an increased caloric intake. One of the most significant changes found in Western diet–fed *Fut2*$^{-/-}$ mice is bile acid metabolism. Plasma bile acids, including both primary and secondary bile acids, had been shown to induce energy expenditure in brown adipose tissue.[47] The most well-studied molecular mechanism that mediates the effects of bile acids on thermogenesis is G-protein–coupled bile acid receptor 1 (also known as takeda-G-protein-receptor-5 [TGR5]). However, we could not detect differences in TGR5 or differences of gastrointestinal hormones associated with appetite and energy expenditures, including glucagon-like peptide-1, peptide YY, and neuropeptide Y between Western diet–fed WT and *Fut2*$^{-/-}$ mice (data not shown). The observed increase in body temperature and activities likely was caused by an unknown mechanism, such as an altered set point of body temperature and emotional or behavioral changes, rather than by changes in bile acid metabolism. Further studies are needed to investigate the underlying mechanisms possibly linking other mechanisms to increased energy expenditure and thermogenesis in *Fut2*-deficient mice.

In summary, *Fut2* deficiency protects mice from diet-induced features of the metabolic syndrome through increased energy expenditure, thermogenesis, and modified microbial metabolism of bile acids. α1-2-fucosylation is an important host-derived regulator of intestinal microbiota and Fut2 plays a critical role for the pathogenesis of obesity and steatohepatitis in mice.

Materials and Methods

All authors had access to the study data and reviewed and approved the final manuscript.

Animal Models

Fut2$^{-/-}$ mice on a C57BL/6 background have been described (kindly provided by Dr Justin Sonnenburg, Stanford University).[17] Heterozygous mice were used for breeding, and WT and *Fut2*$^{-/-}$ littermate mice were used in most experiments. WT C57BL/6 mice were purchased from Charles River (Wilmington, MA) and used in some experiments (Figures 1 and 15). Age-matched 8- to 9-week-old male WT and *Fut2*$^{-/-}$ mice were started on a Western diet (AIN-76A, TestDiet, St. Louis, MO, with a fat content of 20% and energy from fat was 40%), together with glucose (18.9 g/L) and fructose (23.1 g/L) in the drinking water for 20 weeks as described.[57] In Figure 1, Western diet feeding was started at age 6–7 weeks. Control mice received standard chow diet. Mice had free access to food and water. Calorie-restricted *Fut2*$^{-/-}$ mice were provided the same amount of calories daily as their WT littermates on a Western diet. As previously described,[20,21] WT and *Fut2*$^{-/-}$ mice fed a Western diet for 12–13 weeks were gavaged with vancomycin (4 mg/kg body weight [BW]), ampicillin (8 mg/kg BW), neomycin (8 mg/kg BW), metronidazole (8 mg/kg BW), and gentamicin (8 mg/kg BW) for 5 weeks. Control vehicle mice were gavaged with the same amount of water. The gavage was performed twice daily 5 d/wk and once daily 2 d/wk. All antibiotics were purchased from Sigma-Aldrich (St. Louis, MO). Supplementation of 2'-FL (Jennewein Biotechnologie GmbH, Rheinbreitbach, Germany) or L-fucose (GOLDBIO, St. Louis, MO) was performed by adding either of them in the drinking water at a final concentration of 2 g/L. For all in vivo experiments, tissues were harvested from nonfasted mice with the exception of an insulin tolerance test for which mice were fasted for 7 hours, and the bile acid pool and FXR activity study, for which mice were fasted for 4–5 hours.

Insulin Tolerance Test

For the insulin tolerance test, mice were given an intraperitoneal injection of 1 U/kg insulin after 19 weeks on

a Western diet; blood glucose concentrations were measured after 7 hours of fasting before insulin injection, as well as 15, 30, 60, 90, and 120 minutes after injection.

Metabolic Caging

One week before being sacrificed, mice were housed in the Comprehensive Lab Animal Monitoring System

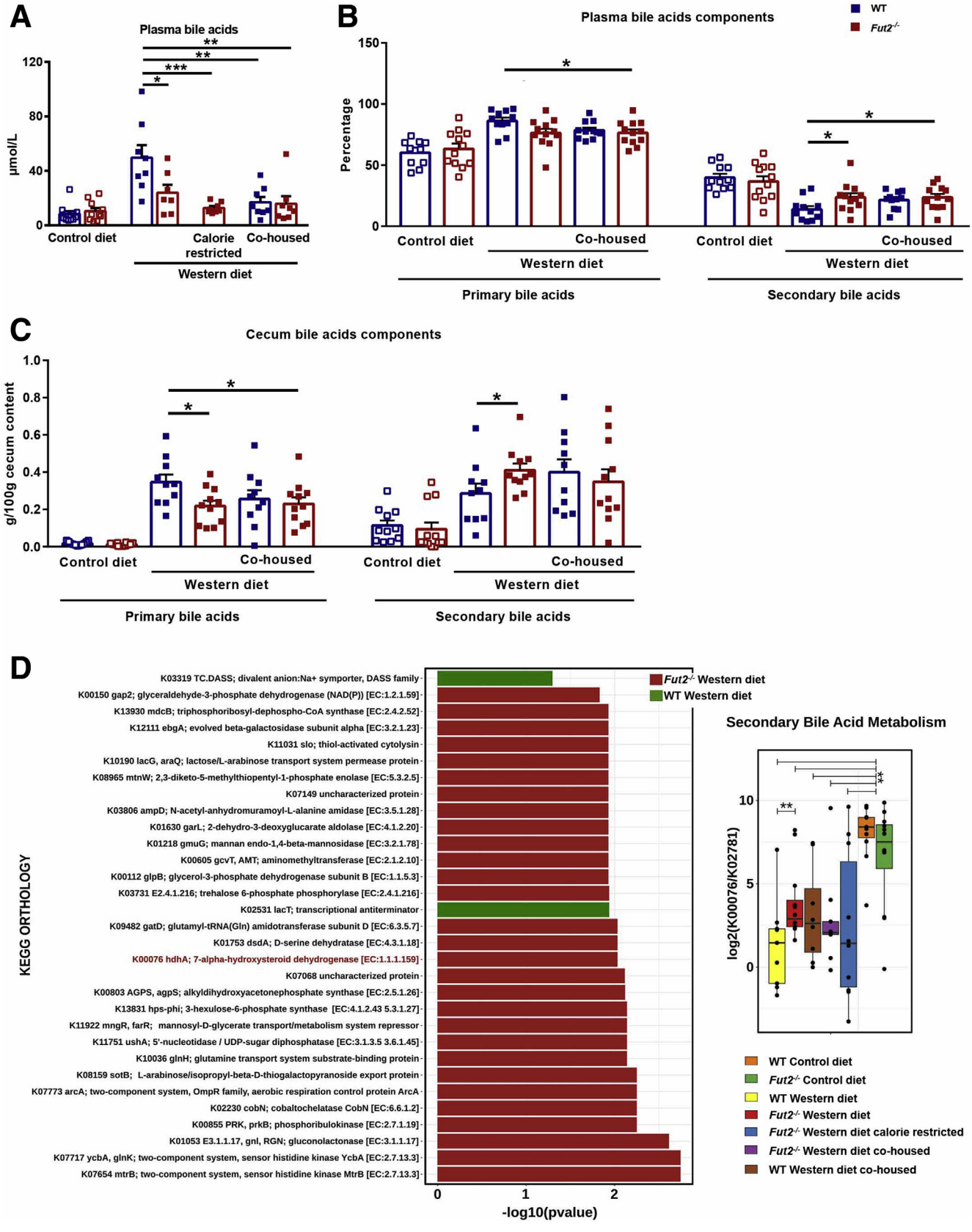

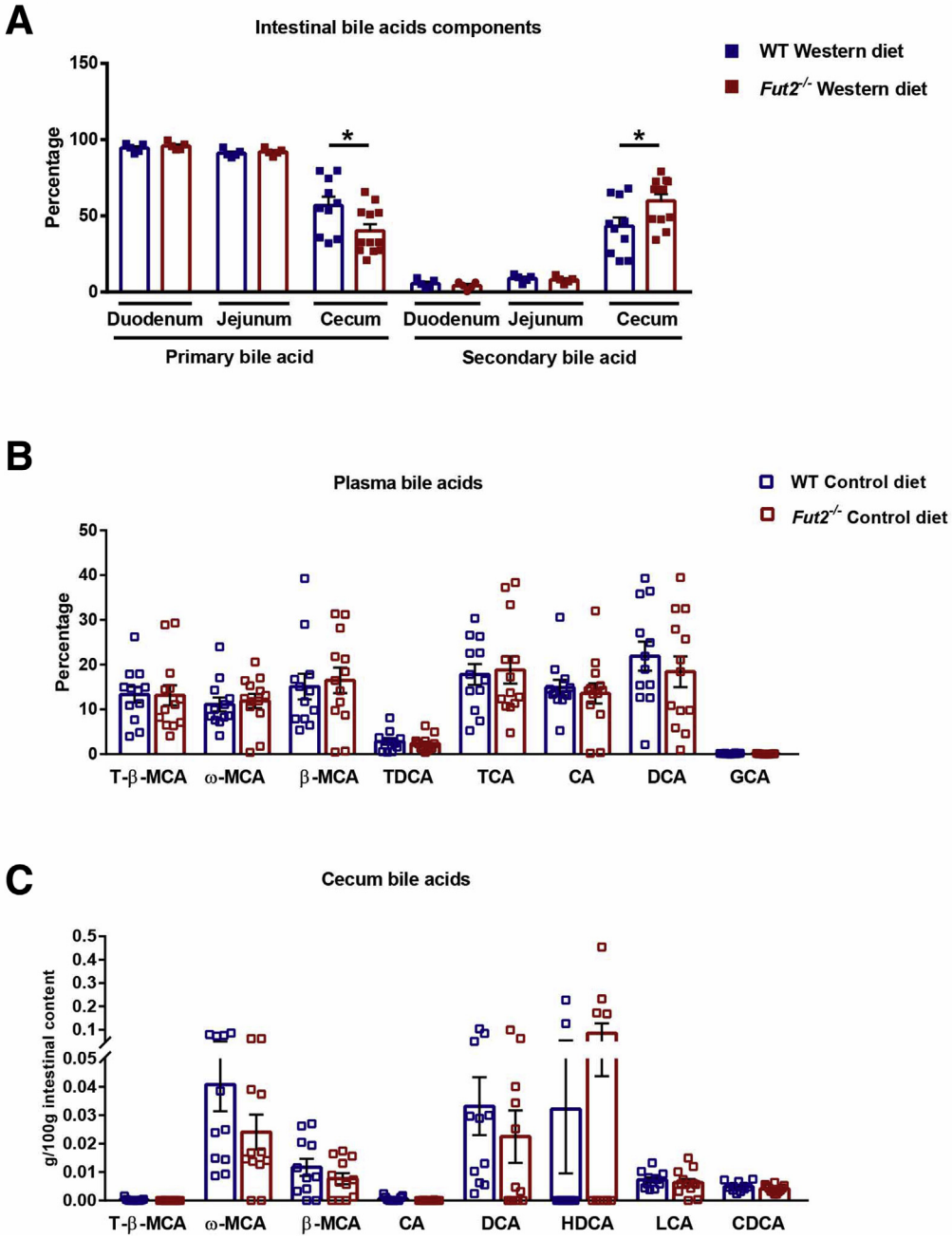

Figure 11. Bile acid composition. *Fut2*$^{-/-}$ and WT littermates were fed with either a control diet or a Western diet for 20 weeks. (*A*) Proportion of primary and secondary bile acids in small (duodenum and jejunum) and large intestine (cecum) in Western diet–fed mice. (*B*) Plasma bile acid composition in control diet–fed mice. (*C*) Cecum bile acid composition in control diet–fed mice. Experiments were performed in n = 10–13 per group from 3–5 experiments. The Student unpaired *t* test was used. Data represent means ± SEM. *$P < .05$.

Figure 10. (***See previous page***). ***Fut2*-deficient mice have altered plasma metabolome and intestinal microbiota.** *Fut2*$^{-/-}$ and WT littermates were fed with either a control diet or a Western diet for 20 weeks. Western diet–fed *Fut2*$^{-/-}$ mice had a significantly higher caloric intake than WT littermate mice and we restricted the total caloric intake of *Fut2*$^{-/-}$ mice to make it equal to the caloric intake of WT mice during Western diet feeding (calorie-restricted group). To facilitate fecal microbiota transfer between mice, freshly weaned WT and *Fut2*$^{-/-}$ mice were co-housed in the same cage and subjected to Western diet feeding. Plasma and cecum contents were collected for targeted metabolomics of bile acids. (*A*) Plasma bile acid levels. (*B*) Proportion of primary and secondary bile acids in plasma. (*C*) Proportion of primary and secondary bile acids in cecum. (*D*) Genomic DNA from mouse feces was extracted and purified for shotgun metagenomic sequencing. Total reads were analyzed using mouse catalog genes.[63] Relative abundance of several bacterial genes and relative abundance of the K00076 (*hsdh*) gene in different groups. For comparisons of relative abundance, a log-ratio of counts was compared using the Kegg Onthology K02781 (carbohydrate metabolism) as the reference frame.[70] Data represent means ± SEM. *$P < .05$, **$P < .01$, and ***$P < .001$. (*A–C*) One-way analysis of variance followed by the Tukey post hoc test was used for comparison between Western diet groups. Experiments were performed in n = 10–13 per group from 3 experiments. (*D*) The Wilcoxon rank sum test was used for comparison between Western diet groups.

(Columbus Instruments, Columbus, OH) for approximately 60 hours to measure VO_2 (mL/kg/min), VCO_2 (mL/kg/min), respiratory exchange ratio (VCO_2/VO_2), heat production (kcal/kg/min; calculated as $VO_2 \times [3.815 + (1.232 \times$ respiratory exchange ratio)]) and activity (infrared beam breaks in the x and y planes) as previously described.[58] All mice had free access to food and water while in metabolic cages.

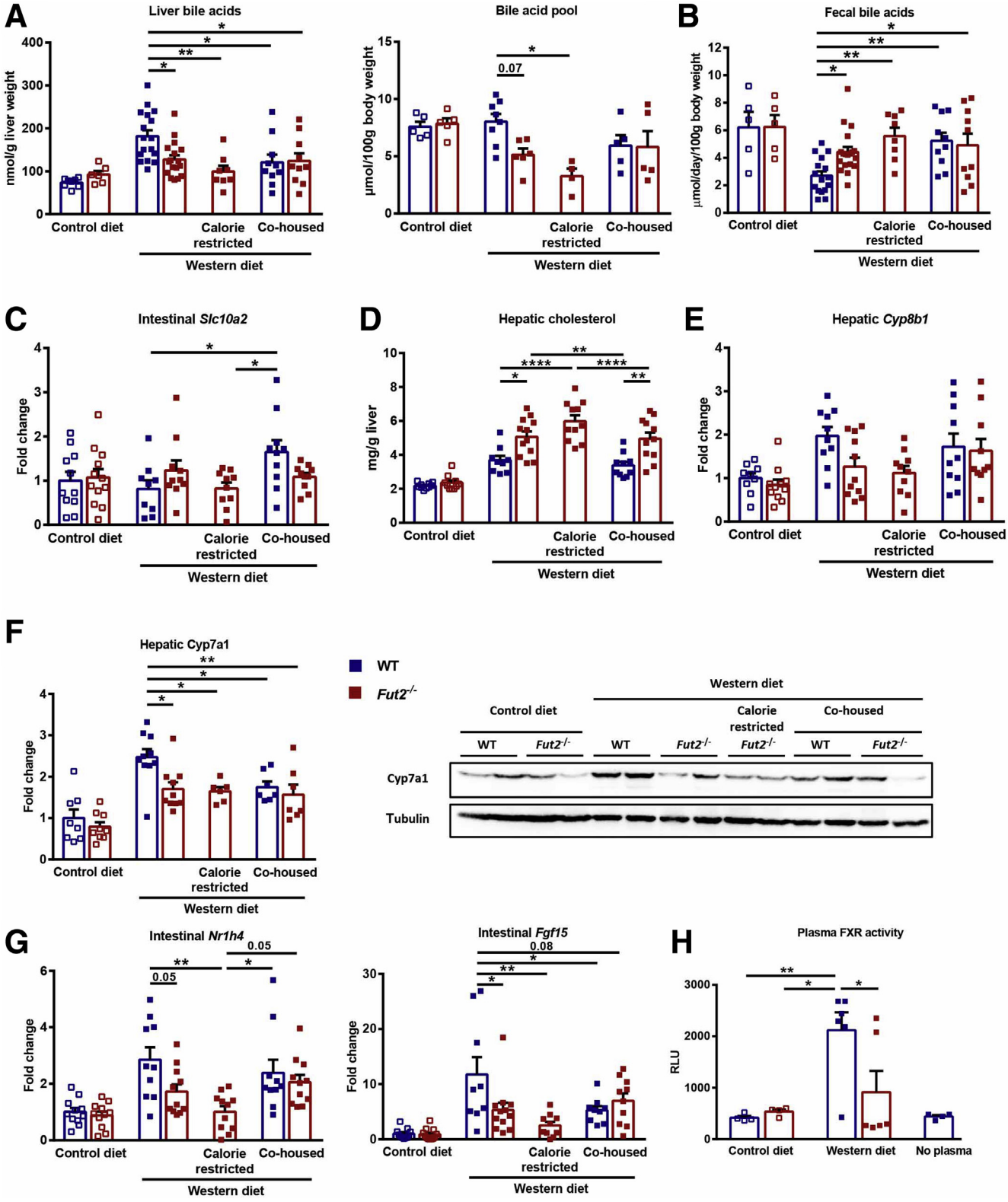

Biochemical Assays

Levels of plasma ALT were measured using the Infinity ALT kit (Thermo Scientific, Waltham, MA). Plasma and hepatic triglyceride and cholesterol levels were measured using the Triglyceride Liquid Reagents Kit (Pointe Scientific, Canton, MI) and Cholesterol Liquid Reagents kit (Pointe Scientific), respectively. Plasma levels of leptin were measured using the mouse leptin enzyme-linked immunosorbent assay kit according to the manufacturer's protocol (Crystal Chem, Elk Grove Village, IL). Total bile acids and the bile acid pool were quantified using a Mouse Total Bile Acid Kit (Crystal Chem) as described.[59] For the total bile acid pool, total liver bile acids, total gallbladder bile acids, and total bile acids from the small intestine and cecum, contents were measured and calculated per gram of body weight.

Staining Procedures

Formalin-fixed and paraffin-embedded livers were stained with H&E (Leica Biosystems, Inc, Buffalo Grove, IL) or 0.1% picrosirius red (Sigma-Aldrich) using standard staining protocols. Sirius red–positive area was quantitated by image analysis software ImageJ (National Institutes of Health, Bethesda, MD). The colon sections were treated with 0.1% H_2O_2 (Sigma-Aldrich) for 30 minutes and blocked with avidin and biotin (Vector, Torrance, CA) for 15 minutes each. After blocking with 1% bovine serum albumin for 5 minutes, colon sections were incubated with biotinylated Ulex Europaeus Agglutinin I (Vector) or biotinylated Aleuria Aurantia Lectin (Vector) overnight at 4°C. Sections then were incubated with streptavidin, horseradish peroxidase for 30 minutes, and followed by 3, 3'-diaminobenzidine solution (Vector) for 2 minutes and hematoxylin for 1 minute.

Real-Time Reverse-Transcription Quantitative PCR

RNA was extracted from mouse tissues, and complementary DNA was generated as described.[60] Quantitative PCR was performed with iTaq universal SYBR Green Supermix (Bio-Rad, Hercules, CA) using a StepOnePlus thermocycler real-time PCR system. Primer sequences for mouse genes were obtained from the National Institutes of Health qPrimerDepot and are listed in Table 1. The values of mouse gene expression were normalized to 18S.

Immunoblotting

Liver or brown adipose tissue were homogenized in RIPA buffer, supplemented with protease inhibitor, and used for immunoblotting. Immunoblot analysis was performed using anti-Cyp7a1 (Abcam, Cambridge, MA), anti-Ucp1 (Abcam), and anti-tubulin (Santa Cruz, Santa Cruz, CA) antibodies. Densitometry of immunoblot analysis was performed using ImageJ software (National Institutes of Health).

Cell Luciferase Assay

For luciferase assay, FXRE-Luc plasmids (FXR responsive element) were transfected into CV1 cells. Plasma was diluted with culture medium with a final concentration of 10% in volume and added to the cell culture. Luciferase activities were measured using a dual-luciferase reporter kit (Promega, Madison, WI) as previously reported.[61]

Shotgun Metagenomic Sequencing

DNA sequencing. Total genomic DNA from mouse feces was extracted using the DNeasy PowerSoil Kit (Qiagen, Valencia, CA) following the manufacturer's instructions as described.[23] Purified DNA was prepared for shotgun metagenomic sequencing using the Nextera XT library (Illumina, San Diego, CA) preparation method with 2 rounds of 0.7× ratio bead-based size selection on an Apollo 324 liquid handler (Takara Bio USA, Mountain View, CA) to generate an average fragment size of 800 base pairs (bp). Libraries were quality-assessed using quantitative PCR and a Bioanalyzer (Agilent Technologies, Santa Clara, CA), and subsequently sequenced on a NovaSeq 6000 S2 flow cell using a 300 cycle (2 × 150 bp) kit, loading 400 pmol/L of pooled library with 1% spike-in of ϕX174 DNA. The target sequencing depth was 5 Gbp (giga-base pair) per sample.

Data analysis. An average of 29.6 million reads were generated per library. Adapters were trimmed from the Illumina data using Trimmomatic v0.36.[62] Samples were filtered of possible mouse contamination by aligning the trimmed reads against reference databases using Bowtie2 v2-2.2.3[63] with the following parameters (-D 20 -R 3 -N 1 -L 20 –very-sensitive-local).

For functional analysis, we used a previously constructed mouse gut microbiome database, comprising approximately 2.6 million nonredundant genes.[23] Non–mouse trimmed reads were aligned to the mouse catalog genes using Bowtie (–very-sensitive) with an average

Figure 12. (***See previous page***). **Effects of *Fut2* deficiency on bile acid metabolism.** *Fut2*$^{-/-}$ and WT littermates were fed with either a control diet or a Western diet for 20 weeks. Western diet–fed *Fut2*$^{-/-}$ mice had a significantly higher caloric intake than WT littermate mice and we restricted the total caloric intake of *Fut2*$^{-/-}$ mice to make it equal to the caloric intake of WT mice during Western diet feeding (calorie-restricted group). To facilitate fecal microbiota transfer between mice, freshly weaned WT and *Fut2*$^{-/-}$ mice were co-housed in the same cage and subjected to Western diet feeding. (*A*) Liver bile acid levels and the total bile acid pool were calculated by adding the total amount of gallbladder, intestinal, and liver bile acids together. (*B*) Fecal bile acid levels. (*C*) Intestinal *Slc10a2* mRNA levels. (*D*) Hepatic cholesterol levels. (*E*) Hepatic *Cyp8b1* mRNA levels. (*F*) Immunoblot for Cyp7a1 in liver tissue. (*G*) Ileum *Nr1h4* and *Fgf15* mRNA levels. (*H*) Plasma FXR activity. Data represent means ± SEM. **P* < .05, ***P* < .01, and *****P* < .0001. One-way analysis of variance followed by the Tukey post hoc test was used for comparison between Western diet groups. Experiments were performed in n = 10–13 per group from 3 experiments. For the FXR activities assay there were n = 4–6 per group, and for the immunoblot there were n = 6–10 per group, and both were from 2 experiments.

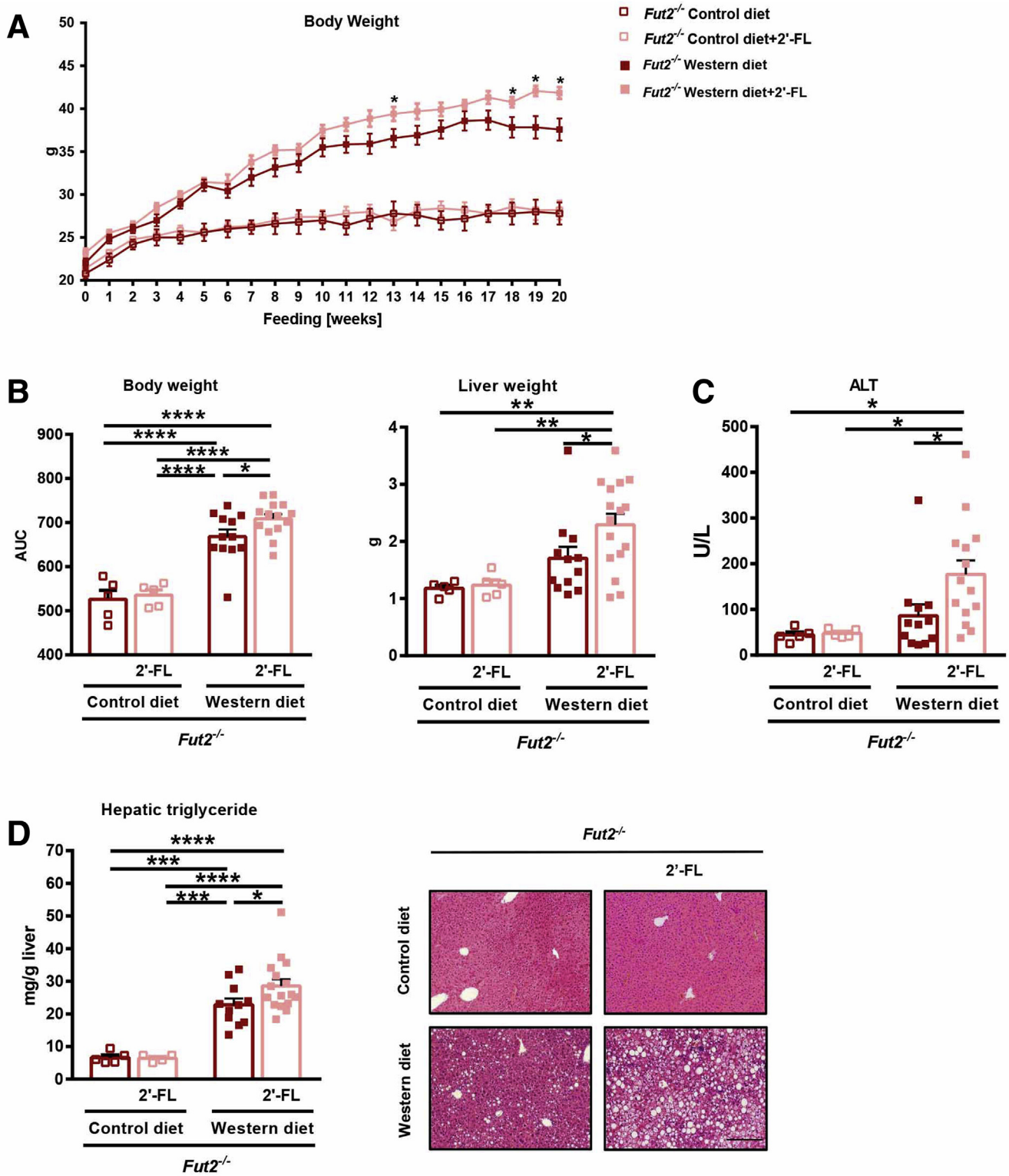

Figure 13. Restoration of α1-2-fucosylation in the intestine exacerbates diet-induced steatohepatitis in *Fut2*-deficient mice. *Fut2*$^{-/-}$ mice were assigned to the 2'-FL–treated group and control group, and fed with either a Western diet or a control diet. In the 2'-FL–treated group, 2'-FL (2 g/L) was supplemented continuously in drinking water. The experimental diet and 2'-FL treatment lasted for 20 weeks. (*A*) Body weight increase during 20 weeks. (*B*) Body weight and liver weight. (*C*) Plasma ALT levels. (*D*) Hepatic triglycerides and H&E-stained liver tissue. Data represent means ± SEM. **P* < .05, ***P* < .01, ****P* < .001, and *****P* < .0001. (*A*) The Student unpaired *t* test was used for comparison between 2 Western diet groups with or without 2'-FL feeding. (*B–D*) One-way analysis of variance followed by the Tukey post hoc test was used for comparison between different groups. *Scale bar*: 200 μm. Experiments were performed in n = 12–16 per group from 3 experiments in Western diet groups and in n = 4–5 per group from 2 experiments in control diet groups. AUC, area under the curve.

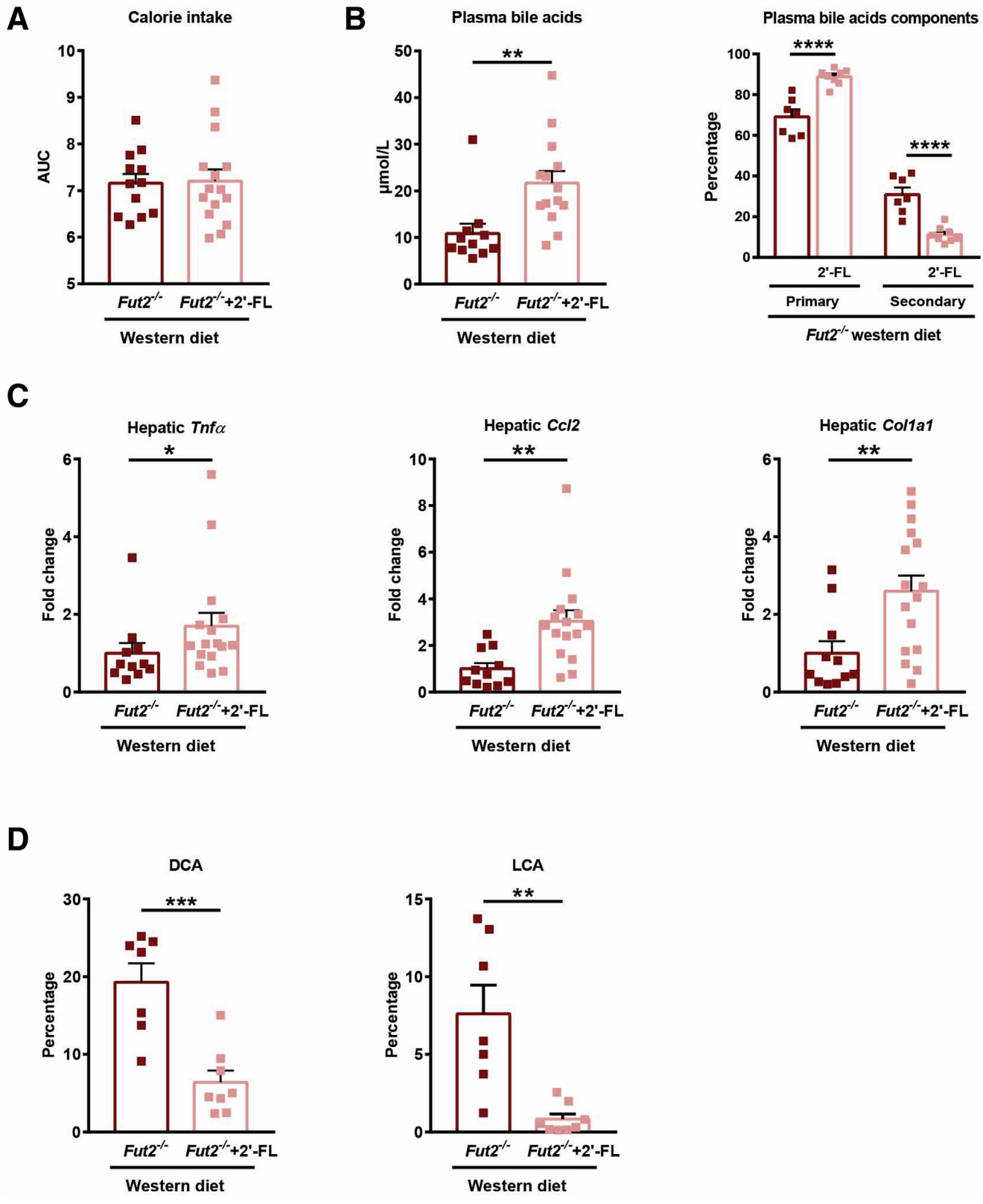

Figure 14. Restoration of α1-2-fucosylation in the intestine exacerbates diet-induced steatohepatitis in *Fut2*-deficient mice. *Fut2*$^{-/-}$ mice were assigned to the 2'-FL–treated group and the control group, and fed with either a Western diet or a control diet. In the 2'-FL–treated group, 2'-FL (2 g/L) was supplemented continuously in drinking water. The experimental diet and the 2'-FL treatment lasted for 20 weeks. (*A*) Calorie intake. (*B*) Plasma bile acid levels and proportion of primary and secondary bile acids in plasma. (*C*) Hepatic *Tnfα*, *Ccl2*, and *Col1a1* mRNA levels. (*D*) Relative amount of DCA and lithocholic acid (LCA) in total plasma bile acids. Data represent means ± SEM. *$P < .05$, **$P < .01$, ***$P < .001$, and ****$P < .0001$. The Student unpaired *t* test was used. Experiments were performed in n = 5–16 per group from 2–3 experiments. AUC, area under the curve.

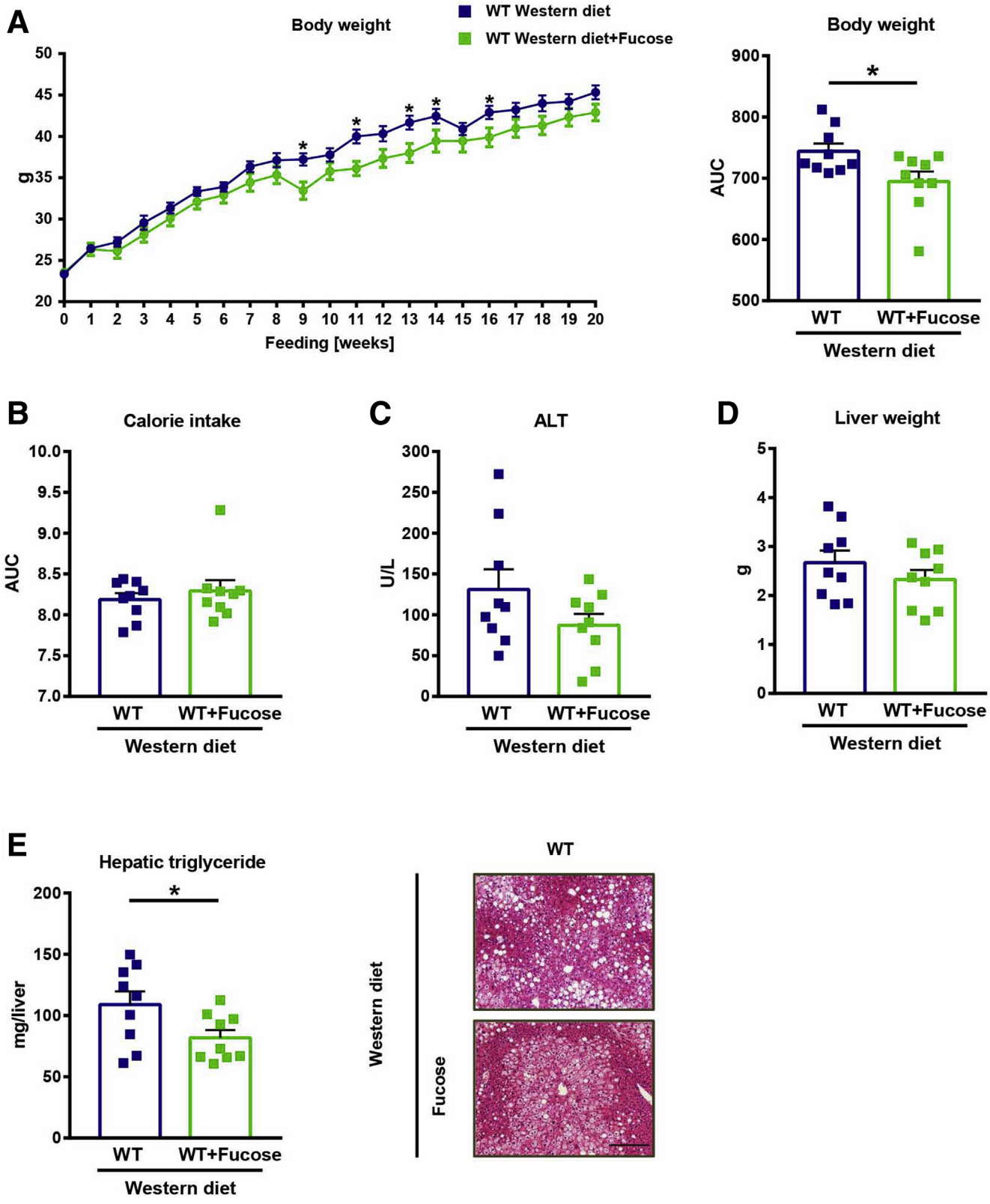

Figure 15. Fucose feeding in WT Western diet–fed mice attenuates body weight increase. WT mice were assigned to L-fucose supplementation or control group, and fed with a Western diet for 20 weeks. In the L-fucose–treated group, L-fucose (2 g/L) was added continuously into the drinking water. (*A*) Body weight. (*B*) Area under curve (AUC) of calorie intake over the course of the experiment. (*C*) Plasma ALT levels. (*D*) Liver weight. (*E*) Hepatic triglyceride levels and representative images of H&E-stained liver tissue. Data represent means ± SEM. *$P < .05$. The Student unpaired *t* test was used. *Scale bar*: 200 μm. Experiments were performed in n = 9 per group from 2 experiments.

Table 1. Sequences of Quantitative PCR Primers

Gene	Primer	Sequence
Mouse 18S	F	5'-AGTCCCTGCCCTTTGTACACA-3'
	R	5'-CGATCCCAGGGCCTCACTA-3'
Mouse Fut2	F	5'-GGTGGATGATGGTGGAAGTC-3'
	R	5'-TTCCCTGTTACCACAGCCAG-3'
Mouse Fut4	F	5'-AAATCCCTATTCCCCTGTGG-3'
	R	5'-CCAGGGGAAGGAAGGTAAAG-3'
Mouse Fut8	F	5'-TGCTTGAATCTGGGTCTTGA-3'
	R	5'-GGCCCTGGTAGTGTTTTCAT-3'
Mouse Tnfα	F	5'-AGGGTCTGGGCCATAGAACT-3'
	R	5'-CCACCACGCTCTTCTGTCTAC-3'
Mouse Ccl2	F	5'-ATTGGGATCATCTTGCTGGT-3'
	R	5'-CCTGCTGTTCACAGTTGCC-3'
Mouse Acta2	F	5'-GTTCAGTGGTGCCTCTGTCA-3'
	R	5'-ACTGGGACGACATGGAAAAG-3'
Mouse Tgfb1	F	5'-GGAGAGCCCTGGATACCAAC-3'
	R	5'-CAACCCAGGTCCTTCCTAAA-3'
Mouse Nr1h4	F	5'-GAAACTGAACATCGGGGTTAT-3'
	R	5'-CGGCGGAGATTTTCAATAAG-3'
Mouse Fgf15	F	5'-GAGGACCAAAACGAACGAAATT-3'
	R	5'-ACGTCCTTGATGGCAATCG-3'
Mouse Col1a1	F	5'-TAGGCCATTGTGTATGCAGC-3'
	R	5'-ACATGTTCAGCTTTGTGGACC-3'
Mouse Slc10a2	F	5'-TGGTGTAGACGAAGAGGCAA-3'
	R	5'-GCCTATTGGATAGATGGCGA-3'
Mouse Cyp8b1	F	5'-CATGGCTTTCCGGAAGAATA-3'
	R	5'-TCTTAATGATGGGGCCAAAG-3'

F, forward; R, reverse.

mapping efficiency of 89.3%. To search for bile acid enzymes associated to bile acid metabolism, enzyme numbers (enzyme commission number, EC number) were used to select their correspondent Kegg Onthology using the KEGG: Kyoto Encyclopedia of Genes and Genomes database (available from https://www.genome.jp/kegg).

For de novo genome assembling, overlapped reads were merged using Flash version 1.2.11.[64] Because of the massive number of reads, the libraries were rarefied to 4 million reads. Merged and unmerged reads were assembled using Spades v3.12.0[65] with the following parameters (-k 25 –meta –merge). Differential binning was performed using MetaBat2 v2.12.1,[66] with minimum contig length of 1500 bp. Bin quality (completeness and contamination) was evaluated using CheckM v1.0.7.[67] Taxonomic classification (closest phylogenetic neighbor) was assessed using RASTtk.[68] In brief, RAST uses a set of unique protein sequences to assign the closest related neighbor. Genome annotations were performed using Prokka v1.11[69] with default parameters.

Microbiome statistical analysis. Microbial diversity was estimated using R package vegan v2.5-2. Plots generated using R package ggplot2 v3.3.2. Differential relative abundance was compared through a log ratio of the counts through Qurro v0.7.1, with statistical significance evaluated through a nonparametric Wilcoxon rank sum test using R scripts. For comparisons of abundance, a log ratio of counts was compared using the Kegg Onthology K02781 (carbohydrate metabolism) as the reference frame.[70] The choice of the reference frame was made using Songbird tool,[70] a Qiime2 lugin,[71] with the following parameters (–formula "genotype_treatment", –epochs 10000, –differential-prior 0.5, –summary-interval 1). Shotgun metagenomic data are available at the Sequence Read Archives BioProject PRJNA614498.

Untargeted Metabolomics of Plasma Samples

Sample preparation. Briefly, 90 μL of methanol/acetonitrile (3:1) solution (containing 0.6 μg/mL L-2-chlorophenylalanine and 6.0 μg/mL ketoprofen as the internal standards) was added to 30 μL plasma and vortexed for 30 seconds. Then, at 4°C, the mixture was centrifuged for protein precipitation (13,000 rpm, 10 min). After that, duplicate supernatants (each for 45 μL) were transferred and dried under nitrogen at room temperature. One of the resulting residues was redissolved in 60 μL of 50% aqueous acetonitrile for untargeted analysis in positive ion mode, while the other was immediately stored at -80°C (for the negative ion mode). Quality control samples were obtained by pooling equal aliquots (10 μL) from each plasma sample and pretreated with the same procedure.

Liquid chromatography-quadrupole-time-of-flight–mass spectrometry analysis. Untargeted analyses were performed using an Agilent 1290 infinity liquid chromatography (LC) system coupled to an Agilent 6545 quadrupole-time-of-flight mass spectrometer (MS) equipped with an electrospray ionization (ESI) source operating in both positive and negative ion modes. Chromatographic separation was evaluated on an Acquity UPLC HSS T3 column (Waters, Wexford, Ireland) (2.1 $\times$ 100 mm, 1.8 μm) with a flow rate of 0.4 mL/min at 50°C. The mobile phase used for ESI^+ consisted of 0.1% aqueous formic acid (mobile phase A) and acetonitrile (mobile phase B). For ESI^-, the mobile phase consisted of (mobile phase A) 10 mmol/L ammonium acetate aqueous solution and (mobile phase B) 10 mmol/L ammonium acetate water/acetonitrile (1:9) solution. A linear gradient elution was optimized as follows: 0–1 minute, 1% B; 1–3 minutes, 1%–15% B; 3–5 minutes, 15%–70% B; 5–9 minutes, 70%–85% B; 9–10 minutes, 85%–100% B; 100% B held for 2 minutes, and then back to the initial conditions with 3 minutes for equilibration. The injection volume was 1.5 μL. MS parameters were set as follows: drying gas temperature, 320°C; drying gas flow rate, 8 L/min; nebulizer gas, 35 psi; fragmental voltage, 120 V; and capillary voltage, 3500 V. A full scan from 50 to 1050 m/z was acquired for each sample under the high-resolution mode (extended dynamic range, 2 GHz).

Data analysis. All the acquired spectra were first converted to mz. data format and then the XCMS package (available from http://metlin.scripps.edu/download) of R program was run for data pretreatment including peak

detection discrimination, baseline correction, and nonlinear retention time alignment. Differential metabolic features tentatively were identified based on accurate mass and MS/MS fragments by searching in online databases such as Human Metabolome Database and METLIN (http://metlin.scripps.edu).

Targeted Metabolomics of Plasma Samples

Plasma pretreatment. A 30-μL aliquot of plasma was mixed with 10 μL of internal standards working solution (9 μg/mL of tauro-β-muricholic acid (T-β-MCA)-d4, 0.9 μg/mL of ω-MCA-d5, 3.6 μg/mL of β-MCA-d5, 4.5 μg/mL of cholic acid (CA)-d4, 1.8 μg/mL of DCA-d4, 9 μg/mL of TCA-d4, and 45 ng/mL of glycocholic acid (GCA)-d4). Then, 80-μL aliquots of methanol solution were added and vortexed for 2 minutes to extract the bile acids. After centrifugation for 10 minutes at 13,000 rpm, 4°C, 100 μL of supernatant carefully was transferred and dried with continuous nitrogen. Finally, the residue was reconstituted in 60 μL of 50% aqueous acetonitrile solution (containing 0.1% formic acid) and 5 μL was injected for further LC-MS/MS analysis.

LC-MS/MS analysis. Targeted analyses were performed using an LC-20A system coupled to a triple quadrupole mass spectrometer (LC-MS/MS 8050; Shimadzu, Nakagyo Ward, Kyoto, Japan) operating in negative ion mode. The high-performance liquid chromatography (HPLC) separation was achieved on an Acquity UPLC HSS T3 column (2.1 × 100 mm, 1.8 μm) maintained at 45°C. Pure water and water/acetonitrile (v/v = 1:9) both containing 1 mmol/L ammonium acetate were used as mobile phase A and B, respectively, at a flow rate of 0.4 mL/min. The gradient elution program was 5%–25% B at 0–1 minute, 25%–30% B at 1–9 minutes, 30%–40% B at 9–10 minutes, 40%–45% B at 10–17 minutes, 45%–95% B at 17–18.5 minutes, and 95% B held for 2 minutes, and then back to the initial conditions with 3 minutes for equilibration. The ESI source parameters were as follows: nebulizing gas flow, 3 L/min; heating gas flow, 10 L/min; drying gas flow, 10 L/min; interface temperature, 300°C; DL temperature, 250°C; and heat block temperature, 400°C.

Targeted quantification. A total of 10 bile acids in plasma were measured quantitatively based on a stable isotope-labeled internal standard calibration strategy. Multiple reaction monitoring mode was selected, thus allowing more precise results and the detailed ion transitions monitored were as follows: T-β-MCA, m/z 514→80; T-β-MCA-d4, m/z 518→80; ω-MCA, m/z 407→407; ω-MCA-d5, m/z 412→412; β-MCA, m/z 407→407; β-MCA-d5, m/z 412→412; DCA, m/z 391→391; DCA-d4, m/z 395→395; CA, m/z 407→407; CA-d4, m/z 411→411; TCA, m/z 514→124; TCA-d4, m/z 518→124; GCA, m/z 464→74; GCA-d4, m/z 468→74; TUDCA, m/z 498→80; TDCA, m/z 498→80; and THDCA, m/z 498→80. Standard solutions over a wide concentration range of 800-fold were prepared for the linearity investigation. All the standard curves showed good linearity with regression coefficients $r^2 >$ 0.99. The accuracy was assessed at high, moderate, and low concentration levels and calculated as recoveries ranged from 80% to 120%, indicating high accuracy of the LC-MS/MS approach. The interday precision (1 replicate of quality control sample analyzed on each of 3 days) and intraday precision (3 replicates analyzed on the same day) also were measured and calculated from the relative SD (RSD, % = SD of peak area ratio/mean of peak area ratio × 100). All the bile acid metabolites with intraday and interday precision (RSD) less than 8% and 15.0%, respectively, further confirmed the stability of the analytical platform. The lower limit of quantification was determined at a signal-to-noise ratio greater than 10.

Targeted Metabolomics of Cecum Content Samples

Sample preparation. Cecum contents were homogenized and dried in a vacuum centrifuge at 37°C until the weight was stable. Fifteen milligrams of homogenized intestinal content was extracted in 1.0 mL 75% ethanol for 1 hour. The extracts were centrifuged at 16,200 × g at 4°C for 10 minutes subsequently. Once the supernatants were prepared, an aliquot of a 900-μL sample of the supernatant was evaporated to dryness under reduced pressure at 45°C using the EZ2 Plus Solvent Evaporation Station (SP Scientific, Warminster, PA). The residue was dissolved by addition of 200 μL acetonitrile and the supernatant was injected into the HPLC–MS/MS system for analysis.

LC-MS/MS analysis. Targeted analyses were performed using an LC-20A system coupled to a triple quadrupole mass spectrometer (LC-MS/MS 8050; Shimadzu) operating in negative ion mode. The HPLC separation was achieved on an Acquity UPLC BEH C18 column (2.1 mm × 100 mm, 1.7 μm) maintained at 45°C. Pure water and water/acetonitrile (v/v = 1:9) both containing 0.1% formic acid were used as mobile phase A and B, respectively, at a flow rate of 0.3 mL/min. The gradient elution program was 30%–65% B at 0–3 minutes, 65%–70% B at 3–10 minutes, 65%–70% B at 10–12 minutes, 70%–85% B at 12–13 minutes, and 85%–30% B at 13–14 minutes. The ESI source parameters were as follows: nebulizing gas flow, 3 L/min; heating gas flow, 10 L/min; drying gas flow, 10 L/min; interface temperature, 300°C; DL temperature, 250°C; and heat block temperature, 400°C.

Targeted quantification. A total of 12 bile acids in plasma were measured quantitatively based on a stable isotope-labeled internal standard calibration strategy. The multiple reaction monitoring mode was selected, thus allowing more precise results and the detailed ion transitions monitored were as follows: T-β-MCA, m/z 514→80; T-β-MCA-d4, m/z 518→80; ω-MCA, m/z 407→407; ω-MCA-d5, m/z 412→412; β-MCA, m/z 407→407; β-MCA-d5, m/z 412→412; DCA, m/z 391→391; DCA-d4, m/z 395→395; CA, m/z 407→407; CA-d4, m/z 411→411; TCA, m/z 514→124; TCA-d4, m/z 518→124; GCA, m/z 464→74; GCA-d4, m/z 468→74; tauroursodeoxycholic acid (TUDCA), m/z 498→80; TDCA, m/z 498→80; and taurohyodeoxycholic acid (THDCA), m/z 498→80; hyodeoxycholic acid (HDCA), m/z 391→391; and chenodeoxycholic acid (CDCA), m/z 391→391. Standard

solutions over a wide concentration range were prepared for the linearity investigation. All of the standard curves showed good linearity with regression coefficients $r^2 > 0.99$. The accuracy was assessed at high, moderate, and low concentration levels and calculated as recoveries ranged from 80% to 120%, indicating high accuracy of the LC-MS/MS approach. The interday precision (1 replicate of quality control sample analyzed on each of 3 days) and intraday precision (3 replicates analyzed on the same day) also were measured and calculated from the RSD (% = SD of peak area ratio/mean of peak area ratio × 100). All the bile acid metabolites with intraday and interday precision (RSD) less than 8% and 15.0%, respectively, further confirmed the stability of the analytic platform. The lower limit of quantification was determined at a signal-to-noise ratio > 10.

Statistical Analysis

All data were expressed as means ± SEM unless otherwise specified. For comparison of 2 groups, the Student unpaired *t* test was used. For comparisons of more than 2 groups, 1-way analysis of variance was used followed by the Tukey post hoc test. Analysis of metabolomic data was performed with R (V.3.5.1; 2018 the R Foundation for Statistical Computing), and principal component analysis and hierarchical cluttering of metabolomics data were performed using MetaboAnalyst 4.0. All the other analyses were performed with GraphPad Prism V.7.0. (La Jolla, CA). A *P* value less than .05 was considered significant.

References

1. Yki-Jarvinen H. Non-alcoholic fatty liver disease as a cause and a consequence of metabolic syndrome. Lancet Diabetes Endocrinol 2014;2:901–910.
2. Younossi ZM, Koenig AB, Abdelatif D, Fazel Y, Henry L, Wymer M. Global epidemiology of nonalcoholic fatty liver disease-meta-analytic assessment of prevalence, incidence, and outcomes. Hepatology 2016;64:73–84.
3. Anstee QM, Targher G, Day CP. Progression of NAFLD to diabetes mellitus, cardiovascular disease or cirrhosis. Nat Rev Gastroenterol Hepatol 2013;10:330–344.
4. Cotter TG, Rinella M. NAFLD 2020: the state of the disease. Gastroenterology 2020;158:1851–1864.
5. Adams LA, Lymp JF, St Sauver J, Sanderson SO, Lindor KD, Feldstein A, Angulo P. The natural history of nonalcoholic fatty liver disease: a population-based cohort study. Gastroenterology 2005;129:113–121.
6. Wree A, Broderick L, Canbay A, Hoffman HM, Feldstein AE. From NAFLD to NASH to cirrhosis-new insights into disease mechanisms. Nat Rev Gastroenterol Hepatol 2013;10:627–636.
7. Kolodziejczyk AA, Zheng D, Shibolet O, Elinav E. The role of the microbiome in NAFLD and NASH. EMBO Mol Med 2019;11:e9302.
8. Domino SE, Zhang L, Lowe JB. Molecular cloning, genomic mapping, and expression of two secretor blood group alpha (1,2)fucosyltransferase genes differentially regulated in mouse uterine epithelium and gastrointestinal tract. J Biol Chem 2001;276:23748–23756.
9. Goto Y, Obata T, Kunisawa J, Sato S, Ivanov II, Lamichhane A, Takeyama N, Kamioka M, Sakamoto M, Matsuki T, Setoyama H, Imaoka A, Uematsu S, Akira S, Domino SE, Kulig P, Becher B, Renauld JC, Sasakawa C, Umesaki Y, Benno Y, Kiyono H. Innate lymphoid cells regulate intestinal epithelial cell glycosylation. Science 2014;345:1254009.
10. Bode L. Human milk oligosaccharides: prebiotics and beyond. Nutr Rev 2009;67(Suppl 2):S183–S191.
11. Bry L, Falk PG, Midtvedt T, Gordon JI. A model of host-microbial interactions in an open mammalian ecosystem. Science 1996;273:1380–1383.
12. Kashyap PC, Marcobal A, Ursell LK, Smits SA, Sonnenburg ED, Costello EK, Higginbottom SK, Domino SE, Holmes SP, Relman DA, Knight R, Gordon JI, Sonnenburg JL. Genetically dictated change in host mucus carbohydrate landscape exerts a diet-dependent effect on the gut microbiota. Proc Natl Acad Sci U S A 2013;110:17059–17064.
13. Goto Y, Uematsu S, Kiyono H. Epithelial glycosylation in gut homeostasis and inflammation. Nat Immunol 2016;17:1244–1251.
14. Lin B, Hayashi Y, Saito M, Sakakibara Y, Yanagisawa M, Iwamori M. GDP-fucose: beta-galactoside alpha1,2-fucosyltransferase, MFUT-II, and not MFUT-I or -III, is induced in a restricted region of the digestive tract of germ-free mice by host-microbe interactions and cycloheximide. Biochim Biophys Acta 2000;1487:275–285.
15. Umesaki Y, Sakata T, Yajima T. Abrupt induction of GDP-fucose: asialo GM1 fucosyltransferase in the small intestine after conventionalization of germ-free mice. Biochem Biophys Res Commun 1982;105:439–443.
16. Pickard JM, Maurice CF, Kinnebrew MA, Abt MC, Schenten D, Golovkina TV, Bogatyrev SR, Ismagilov RF, Pamer EG, Turnbaugh PJ, Chervonsky AV. Rapid fucosylation of intestinal epithelium sustains host-commensal symbiosis in sickness. Nature 2014;514:638–641.
17. Tong M, McHardy I, Ruegger P, Goudarzi M, Kashyap PC, Haritunians T, Li X, Graeber TG, Schwager E, Huttenhower C, Fornace AJ Jr, Sonnenburg JL, McGovern DP, Borneman J, Braun J. Reprograming of gut microbiome energy metabolism by the FUT2 Crohn's disease risk polymorphism. ISME J 2014;8:2193–2206.
18. Pham TA, Clare S, Goulding D, Arasteh JM, Stares MD, Browne HP, Keane JA, Page AJ, Kumasaka N, Kane L, Mottram L, Harcourt K, Hale C, Arends MJ, Gaffney DJ, Dougan G, Lawley TD. Epithelial IL-22RA1-mediated fucosylation promotes intestinal colonization resistance to an opportunistic pathogen. Cell Host Microbe 2014;16:504–516.
19. Bunesova V, Lacroix C, Schwab C. Fucosyllactose and L-fucose utilization of infant Bifidobacterium longum and Bifidobacterium kashiwanohense. BMC Microbiol 2016;16:248.
20. Zhao S, Jang C, Liu J, Uehara K, Gilbert M, Izzo L, Zeng X, Trefely S, Fernandez S, Carrer A, Miller KD,

Schug ZT, Snyder NW, Gade TP, Titchenell PM, Rabinowitz JD, Wellen KE. Dietary fructose feeds hepatic lipogenesis via microbiota-derived acetate. Nature 2020; 579:586–591.

21. Hartmann P, Seebauer CT, Mazagova M, Horvath A, Wang L, Llorente C, Varki NM, Brandl K, Ho SB, Schnabl B. Deficiency of intestinal mucin-2 protects mice from diet-induced fatty liver disease and obesity. Am J Physiol Gastrointest Liver Physiol 2016; 310:G310–G322.
22. Cani PD, Bibiloni R, Knauf C, Waget A, Neyrinck AM, Delzenne NM, Burcelin R. Changes in gut microbiota control metabolic endotoxemia-induced inflammation in high-fat diet-induced obesity and diabetes in mice. Diabetes 2008;57:1470–1481.
23. Xiao L, Feng Q, Liang S, Sonne SB, Xia Z, Qiu X, Li X, Long H, Zhang J, Zhang D, Liu C, Fang Z, Chou J, Glanville J, Hao Q, Kotowska D, Colding C, Licht TR, Wu D, Yu J, Sung JJ, Liang Q, Li J, Jia H, Lan Z, Tremaroli V, Dworzynski P, Nielsen HB, Backhed F, Dore J, Le Chatelier E, Ehrlich SD, Lin JC, Arumugam M, Wang J, Madsen L, Kristiansen K. A catalog of the mouse gut metagenome. Nat Biotechnol 2015; 33:1103–1108.
24. Ridlon JM, Harris SC, Bhowmik S, Kang DJ, Hylemon PB. Consequences of bile salt biotransformations by intestinal bacteria. Gut Microbes 2016;7:22–39.
25. Doden H, Sallam LA, Devendran S, Ly L, Doden G, Daniel SL, Alves JMP, Ridlon JM. Metabolism of oxo-bile acids and characterization of recombinant 12alpha-hydroxysteroid dehydrogenases from bile acid 7alpha-dehydroxylating human gut bacteria. Appl Environ Microbiol 2018;84:e00235-18.
26. Hylemon PB, Harris SC, Ridlon JM. Metabolism of hydrogen gases and bile acids in the gut microbiome. FEBS Lett 2018;592:2070–2082.
27. Ridlon JM, Kang DJ, Hylemon PB. Bile salt biotransformations by human intestinal bacteria. J Lipid Res 2006;47:241–259.
28. Fukiya S, Arata M, Kawashima H, Yoshida D, Kaneko M, Minamida K, Watanabe J, Ogura Y, Uchida K, Itoh K, Wada M, Ito S, Yokota A. Conversion of cholic acid and chenodeoxycholic acid into their 7-oxo derivatives by Bacteroides intestinalis AM-1 isolated from human feces. FEMS Microbiol Lett 2009;293:263–270.
29. Tawthep S, Fukiya S, Lee JY, Hagio M, Ogura Y, Hayashi T, Yokota A. Isolation of six novel 7-oxo- or urso-type secondary bile acid-producing bacteria from rat cecal contents. J Biosci Bioeng 2017; 124:514–522.
30. Wahlstrom A, Sayin SI, Marschall HU, Backhed F. Intestinal crosstalk between bile acids and microbiota and its impact on host metabolism. Cell Metab 2016; 24:41–50.
31. Jia W, Xie G, Jia W. Bile acid-microbiota crosstalk in gastrointestinal inflammation and carcinogenesis. Nat Rev Gastroenterol Hepatol 2018;15:111–128.
32. Wu G, Niu M, Tang W, Hu J, Wei G, He Z, Chen Y, Jiang Y, Chen P. L-fucose ameliorates high-fat diet-induced obesity and hepatic steatosis in mice. J Transl Med 2018;16:344.
33. Ferrer-Admetlla A, Sikora M, Laayouni H, Esteve A, Roubinet F, Blancher A, Calafell F, Bertranpetit J, Casals F. A natural history of FUT2 polymorphism in humans. Mol Biol Evol 2009;26:1993–2003.
34. Kelly RJ, Rouquier S, Giorgi D, Lennon GG, Lowe JB. Sequence and expression of a candidate for the human secretor blood group alpha(1,2)fucosyltransferase gene (FUT2). Homozygosity for an enzyme-inactivating nonsense mutation commonly correlates with the non-secretor phenotype. J Biol Chem 1995;270:4640–4649.
35. Folseraas T, Melum E, Rausch P, Juran BD, Ellinghaus E, Shiryaev A, Laerdahl JK, Ellinghaus D, Schramm C, Weismuller TJ, Gotthardt DN, Hov JR, Clausen OP, Weersma RK, Janse M, Boberg KM, Bjornsson E, Marschall HU, Cleynen I, Rosenstiel P, Holm K, Teufel A, Rust C, Gieger C, Wichmann HE, Bergquist A, Ryu E, Ponsioen CY, Runz H, Sterneck M, Vermeire S, Beuers U, Wijmenga C, Schrumpf E, Manns MP, Lazaridis KN, Schreiber S, Baines JF, Franke A, Karlsen TH. Extended analysis of a genome-wide association study in primary sclerosing cholangitis detects multiple novel risk loci. J Hepatol 2012;57:366–375.
36. McGovern DP, Jones MR, Taylor KD, Marciante K, Yan X, Dubinsky M, Ippoliti A, Vasiliauskas E, Berel D, Derkowski C, Dutridge D, Fleshner P, Shih DQ, Melmed G, Mengesha E, King L, Pressman S, Haritunians T, Guo X, Targan SR, Rotter JI. Fucosyltransferase 2 (FUT2) non-secretor status is associated with Crohn's disease. Hum Mol Genet 2010; 19:3468–3476.
37. Rausch P, Rehman A, Kunzel S, Hasler R, Ott SJ, Schreiber S, Rosenstiel P, Franke A, Baines JF. Colonic mucosa-associated microbiota is influenced by an interaction of Crohn disease and FUT2 (secretor) genotype. Proc Natl Acad Sci U S A 2011; 108:19030–19035.
38. Rayes A, Morrow AL, Payton LR, Lake KE, Lane A, Davies SM. A genetic modifier of the gut microbiome influences the risk of graft-versus-host disease and bacteremia after hematopoietic stem cell transplantation. Biol Blood Marrow Transplant 2016;22:418–422.
39. Magalhaes A, Gomes J, Ismail MN, Haslam SM, Mendes N, Osorio H, David L, Le Pendu J, Haas R, Dell A, Boren T, Reis CA. Fut2-null mice display an altered glycosylation profile and impaired BabA-mediated Helicobacter pylori adhesion to gastric mucosa. Glycobiology 2009;19:1525–1536.
40. Magalhaes A, Reis CA. Helicobacter pylori adhesion to gastric epithelial cells is mediated by glycan receptors. Braz J Med Biol Res 2010;43:611–618.
41. Ruiz-Palacios GM, Cervantes LE, Ramos P, Chavez-Munguia B, Newburg DS. Campylobacter jejuni binds intestinal H(O) antigen (Fuc alpha 1, 2Gal beta 1, 4GlcNAc), and fucosyloligosaccharides of human milk inhibit its binding and infection. J Biol Chem 2003; 278:14112–14120.
42. Blackwell CC, Jonsdottir K, Hanson M, Todd WT, Chaudhuri AK, Mathew B, Brettle RP, Weir DM. Non-

secretion of ABO antigens predisposing to infection by Neisseria meningitidis and Streptococcus pneumoniae. Lancet 1986;2:284–285.

43. Rupp C, Friedrich K, Folseraas T, Wannhoff A, Bode KA, Weiss KH, Schirmacher P, Sauer P, Stremmel W, Gotthardt DN. Fut2 genotype is a risk factor for dominant stenosis and biliary candida infections in primary sclerosing cholangitis. Aliment Pharmacol Ther 2014; 39:873–882.
44. Maroni L, Hohenester SD, van de Graaf SFJ, Tolenaars D, van Lienden K, Verheij J, Marzioni M, Karlsen TH, Oude Elferink RPJ, Beuers U. Knockout of the primary sclerosing cholangitis-risk gene Fut2 causes liver disease in mice. Hepatology 2017; 66:542–554.
45. Duvallet C, Gibbons SM, Gurry T, Irizarry RA, Alm EJ. Meta-analysis of gut microbiome studies identifies disease-specific and shared responses. Nat Commun 2017;8:1784.
46. Zhou R, Fan X, Schnabl B. Role of the intestinal microbiome in liver fibrosis development and new treatment strategies. Transl Res 2019;209:22–38.
47. Watanabe M, Houten SM, Mataki C, Christoffolete MA, Kim BW, Sato H, Messaddeq N, Harney JW, Ezaki O, Kodama T, Schoonjans K, Bianco AC, Auwerx J. Bile acids induce energy expenditure by promoting intracellular thyroid hormone activation. Nature 2006; 439:484–489.
48. Caussy C, Hsu C, Singh S, Bassirian S, Kolar J, Faulkner C, Sinha N, Bettencourt R, Gara N, Valasek MA, Schnabl B, Richards L, Brenner DA, Hofmann AF, Loomba R. Serum bile acid patterns are associated with the presence of NAFLD in twins, and dose-dependent changes with increase in fibrosis stage in patients with biopsy-proven NAFLD. Aliment Pharmacol Ther 2019; 49:183–193.
49. Mouzaki M, Wang AY, Bandsma R, Comelli EM, Arendt BM, Zhang L, Fung S, Fischer SE, McGilvray IG, Allard JP. Bile acids and dysbiosis in non-alcoholic fatty liver disease. PLoS One 2016;11:e0151829.
50. Labbe A, Ganopolsky JG, Martoni CJ, Prakash S, Jones ML. Bacterial bile metabolising gene abundance in Crohn's, ulcerative colitis and type 2 diabetes metagenomes. PLoS One 2014;9:e115175.
51. Puri P, Daita K, Joyce A, Mirshahi F, Santhekadur PK, Cazanave S, Luketic VA, Siddiqui MS, Boyett S, Min HK, Kumar DP, Kohli R, Zhou H, Hylemon PB, Contos MJ, Idowu M, Sanyal AJ. The presence and severity of nonalcoholic steatohepatitis is associated with specific changes in circulating bile acids. Hepatology 2018; 67:534–548.
52. Ferrell JM, Boehme S, Li F, Chiang JY. Cholesterol 7alpha-hydroxylase-deficient mice are protected from high-fat/high-cholesterol diet-induced metabolic disorders. J Lipid Res 2016;57:1144–1154.
53. Schreuder TC, Marsman HA, Lenicek M, van Werven JR, Nederveen AJ, Jansen PL, Schaap FG. The hepatic response to FGF19 is impaired in patients with nonalcoholic fatty liver disease and insulin resistance. Am J Physiol Gastrointest Liver Physiol 2010; 298:G440–G445.
54. Bechmann LP, Kocabayoglu P, Sowa JP, Sydor S, Best J, Schlattjan M, Beilfuss A, Schmitt J, Hannivoort RA, Kilicarslan A, Rust C, Berr F, Tschopp O, Gerken G, Friedman SL, Geier A, Canbay A. Free fatty acids repress small heterodimer partner (SHP) activation and adiponectin counteracts bile acid-induced liver injury in superobese patients with nonalcoholic steatohepatitis. Hepatology 2013;57:1394–1406.
55. Fu T, Choi SE, Kim DH, Seok S, Suino-Powell KM, Xu HE, Kemper JK. Aberrantly elevated microRNA-34a in obesity attenuates hepatic responses to FGF19 by targeting a membrane coreceptor beta-Klotho. Proc Natl Acad Sci U S A 2012;109:16137–16142.
56. Appleby RN, Moghul I, Khan S, Yee M, Manousou P, Neal TD, Walters JRF. Non-alcoholic fatty liver disease is associated with dysregulated bile acid synthesis and diarrhea: a prospective observational study. PLoS One 2019;14:e0211348.
57. Bluemel S, Wang L, Martino C, Lee S, Wang Y, Williams B, Horvath A, Stadlbauer V, Zengler K, Schnabl B. The role of intestinal C-type regenerating islet derived-3 lectins for nonalcoholic steatohepatitis. Hepatol Commun 2018;2:393–406.
58. Hucik B, Sarr O, Nakamura MT, Dyck DJ, Mutch DM. Reduced delta-6 desaturase activity partially protects against high-fat diet-induced impairment in whole-body glucose tolerance. J Nutr Biochem 2019;67:173–181.
59. Hartmann P, Hochrath K, Horvath A, Chen P, Seebauer CT, Llorente C, Wang L, Alnouti Y, Fouts DE, Starkel P, Loomba R, Coulter S, Liddle C, Yu RT, Ling L, Rossi SJ, DePaoli AM, Downes M, Evans RM, Brenner DA, Schnabl B. Modulation of the intestinal bile acid/farnesoid X receptor/fibroblast growth factor 15 axis improves alcoholic liver disease in mice. Hepatology 2018;67:2150–2166.
60. Wang L, Mazagova M, Pan C, Yang S, Brandl K, Liu J, Reilly SM, Wang Y, Miao Z, Loomba R, Lu N, Guo Q, Liu J, Yu RT, Downes M, Evans RM, Brenner DA, Saltiel AR, Beutler B, Schnabl B. YIPF6 controls sorting of FGF21 into COPII vesicles and promotes obesity. Proc Natl Acad Sci U S A 2019;116:15184–15193.
61. Fu T, Coulter S, Yoshihara E, Oh TG, Fang S, Cayabyab F, Zhu Q, Zhang T, Leblanc M, Liu S, He M, Waizenegger W, Gasser E, Schnabl B, Atkins AR, Yu RT, Knight R, Liddle C, Downes M, Evans RM. FXR regulates intestinal cancer stem cell proliferation. Cell 2019; 176:1098–1112.e18.
62. Bolger AM, Lohse M, Usadel B. Trimmomatic: a flexible trimmer for Illumina sequence data. Bioinformatics 2014; 30:2114–2120.
63. Langmead B, Salzberg SL. Fast gapped-read alignment with Bowtie 2. Nat Methods 2012;9:357–359.
64. Magoc T, Salzberg SL. FLASH: fast length adjustment of short reads to improve genome assemblies. Bioinformatics 2011;27:2957–2963.

65. Nurk S, Meleshko D, Korobeynikov A, Pevzner PA. metaSPAdes: a new versatile metagenomic assembler. Genome Res 2017;27:824–834.
66. Kang DD, Froula J, Egan R, Wang Z. MetaBAT, an efficient tool for accurately reconstructing single genomes from complex microbial communities. PeerJ 2015; 3:e1165.
67. Parks DH, Imelfort M, Skennerton CT, Hugenholtz P, Tyson GW. CheckM: assessing the quality of microbial genomes recovered from isolates, single cells, and metagenomes. Genome Res 2015;25:1043–1055.
68. Brettin T, Davis JJ, Disz T, Edwards RA, Gerdes S, Olsen GJ, Olson R, Overbeek R, Parrello B, Pusch GD, Shukla M, Thomason JA 3rd, Stevens R, Vonstein V, Wattam AR, Xia F. RASTtk: a modular and extensible implementation of the RAST algorithm for building custom annotation pipelines and annotating batches of genomes. Sci Rep 2015;5:8365.
69. Seemann T. Prokka: rapid prokaryotic genome annotation. Bioinformatics 2014;30:2068–2069.
70. Morton JT, Marotz C, Washburne A, Silverman J, Zaramela LS, Edlund A, Zengler K, Knight R. Establishing microbial composition measurement standards with reference frames. Nat Commun 2019;10:2719.
71. Bolyen E, Rideout JR, Dillon MR, Bokulich NA, Abnet CC, Al-Ghalith GA, Alexander H, Alm EJ, Arumugam M, Asnicar F, Bai Y, Bisanz JE, Bittinger K, Brejnrod A, Brislawn CJ, Brown CT, Callahan BJ, Caraballo-Rodriguez AM, Chase J, Cope EK, Da Silva R, Diener C, Dorrestein PC, Douglas GM, Durall DM, Duvallet C, Edwardson CF, Ernst M, Estaki M, Fouquier J, Gauglitz JM, Gibbons SM, Gibson DL, Gonzalez A, Gorlick K, Guo J, Hillmann B, Holmes S, Holste H, Huttenhower C, Huttley GA, Janssen S, Jarmusch AK, Jiang L, Kaehler BD, Kang KB, Keefe CR, Keim P, Kelley ST, Knights D, Koester I, Kosciolek T, Kreps J, Langille MGI, Lee J, Ley R, Liu YX, Loftfield E, Lozupone C, Maher M, Marotz C, Martin BD, McDonald D, McIver LJ, Melnik AV, Metcalf JL, Morgan SC, Morton JT, Naimey AT, Navas-Molina JA, Nothias LF, Orchanian SB, Pearson T, Peoples SL, Petras D, Preuss ML, Pruesse E, Rasmussen LB, Rivers A, Robeson MS 2nd, Rosenthal P, Segata N, Shaffer M, Shiffer A, Sinha R, Song SJ, Spear JR, Swafford AD, Thompson LR, Torres PJ, Trinh P, Tripathi A, Turnbaugh PJ, Ul-Hasan S, van der Hooft JJJ, Vargas F, Vazquez-Baeza Y, Vogtmann E, von Hippel M, Walters W, Wan Y, Wang M, Warren J, Weber KC, Williamson CHD, Willis AD, Xu ZZ, Zaneveld JR, Zhang Y, Zhu Q, Knight R, Caporaso JG. Reproducible, interactive, scalable and extensible microbiome data science using QIIME 2. Nat Biotechnol 2019; 37:852–857.

Received April 17, 2020. Accepted February 16, 2021.

Correspondence
Address correspondence to: Bernd Schnabl, MD, Department of Medicine, University of California San Diego, 9500 Gilman Drive, MC0702, La Jolla, California 92093. e-mail: beschnabl@ucsd.edu.

CRediT Authorship Contributions

Rongrong Zhou (Conceptualization: Supporting; Data curation: Equal; Formal analysis: Lead; Methodology: Lead; Writing – original draft: Lead)

Cristina Llorente (Conceptualization: Lead; Data curation: Equal; Formal analysis: Supporting; Funding acquisition: Supporting; Methodology: Supporting; Writing – review & editing: Lead)

Jingling Cao (Data curation: Supporting; Formal analysis: Supporting; Methodology: Supporting)

Livia S. Zaramela (Data curation: Supporting; Formal analysis: Supporting)

Suling Zeng (Data curation: Supporting)

Bei Gao (Formal analysis: Supporting)

Shang-Zhen Li (Methodology: Supporting)

Ryan D. Welch (Methodology: Supporting)

Feng-Qing Huang (Methodology: Supporting)

Lian-Wen Qi (Methodology: Supporting)

Chuyue Pan (Methodology: Supporting)

Yan Huang (Resources: Supporting)

Pengchen Zhou (Data curation: Supporting)

Iris Beussen (Formal analysis: Supporting)

Ying Zhang (Formal analysis: Supporting)

Gregory Bryam (Formal analysis: Supporting)

Oliver Fiehn (Supervision: Supporting)

Lirui Wang (Resources: Supporting)

E-Hu Liu (Methodology: Supporting)

Ruth T. Yu (Resources: Supporting)

Michael Downes (Writing – review & editing: Supporting)

Ronald M. Evans (Writing – review & editing: Supporting)

Karrie Goglin (Resources: Supporting)

Derrick E. Fouts (Writing – review & editing: Supporting)

David A. Brenner (Supervision: Supporting)

Lars Bode (Data curation: Supporting; Resources: Supporting; Writing – review & editing: Supporting)

Xuegong Fan (Supervision: Supporting)

Karsten Zengler (Data curation: Supporting; Writing – review & editing: Supporting)

Bernd Schnabl, MD (Conceptualization: Lead; Funding acquisition: Lead; Supervision: Lead; Writing – review & editing: Lead)

Conflicts of interest
Bernd Schnabl has consulted for Ferring Research Institute, HOST Therabiomics, Intercept Pharmaceuticals, Patara Pharmaceuticals, Mabwell Therapeutics, and Takeda. The University of California San Diego has received grant support from Axial Biotherapeutics, BiomX, CymaBay Therapeutics, NGM Biopharmaceuticals, and Synlogic Operating Company. The remaining authors disclose no conflicts.

Funding
This study was supported by Hunan Provincial Natural Science Foundation of China grant 2020JJ4932 (R.Z.). Rongrong Zhou's work in the United States is supported by a foundation from Xiangya Hospital of China. The study was supported by an American Association for the Study of Liver Diseases Pinnacle Research Award in Liver Disease and a pilot project award from Southern California Research Center for Alcoholic Liver and Pancreatic Disease and Cirrhosis (P50 AA011999) (C.L.). This study was supported in part by National Institutes of Health grants R01 AA24726, R01AA020703, and U01 AA026939, by award BX004594 from the Biomedical Laboratory Research and Development Service of the VA Office of Research and Development (B.S.), services provided by P30 DK120515 and funding from the Larsson-Rosenquist Foundation Mother-Milk-Infant Center of Research Excellence at UC San Diego (L.B. and B.S.). This study also was supported in part by the National Natural Science Foundation of China grant 81970550 (Y.H.), the National Natural Science Foundation for Young Scientists of China grant 81800472 (P.Z.), and scholarship 20161625 from the Shanxi Scholarship Council of China in 2016 (J.C.).